Coordination Chemistry Reviews 490 (2023) 215213

Contents lists available at ScienceDirect

Coordination Chemistry Reviews

journal homepage: www.elsevier.com/locate/ccr

Review

Electronic structure and magnetic anisotropy design of functional metal complexes

Arsen Raza, Mauro Perfetti *

Department of Chemistry "U. Schiff", University of Florence, Via della Lastruccia 3, 50019 Sesto Fiorentino, Italy

ARTICLE INFO

Keywords:
Single molecule magnets
Pseudo contact shift agents
Magnetic refrigerants
Anisotropy switches
Optically addressable qubits
Magnetic anisotropy
Electronic structure

ABSTRACT

Chemical guidelines to target a well-defined electronic structure and magnetic anisotropy are of primary importance in physics, chemistry and biology. Our literature overview highlights that engineering the energy gap between the ground and first excited state and tailoring the magnetic anisotropy of paramagnetic molecules is an excellent starting point for boosting the performances of many molecular materials with emerging properties of technological relevance such as Single Molecule Magnets, Pseudo Contact Shift agents, Optically Addressable Qubits, Magnetic Refrigerants, and Magnetic Anisotropy Switches. We also discuss the compatibility between different functionalities.

1. Introduction

The electronic structure of a paramagnetic material defines its magnetic properties and stems from a combination of several contributions. Some of them originate from the intrinsic energy level structure of the constituent atoms while others are connected to the chemical structure of the material (*i.e.* the mutual organization of the atoms in it) or to external perturbations such as magnetic fields.

In solid state inorganic materials, the magnetic properties are often related to strong interactions between the magnetic centres that produce magnetic ordering [1–3]. The spatial control over such interactions is pivotal because it can generate magnetic anisotropy, that is the directional dependence of a material's magnetic properties [4–6]. Magnetic anisotropy is at the base of several magnetic phenomena such as magnetic coercivity, with a variety of applications in diverse fields such as mechanical engineering and biophysics [7–9].

Conversely from extended inorganic lattices, the properties of molecular materials, especially of coordination complexes, are predominantly influenced by the single molecule electronic structure, while intermolecular magnetic interactions often play a minor role. This behaviour is essentially dictated by the chemical structure of most coordination compounds. A metal core is surrounded by an organic shell that stabilizes and protects the magnetic properties from external perturbations. This picture stresses the importance of coordination chemistry as the primary tool to create materials with *ad hoc* magnetic properties. Playing with the specific characteristics of the metal ion(s), such as oxidation states and radial extension of the valence orbitals, is key to build up performant materials. Of course, the ligands and their geometry are also extremely important. For instance, a judicious use of coordination chemistry has led to materials with complex magnetic anisotropy structures, from spin chains [10] to 3D spin architectures [11].

In this review we describe how the electronic structure and magnetic anisotropy must be chemically engineered to target five types of functional materials. In Section 2 we briefly present how the electronic structure, and the resultant magnetic anisotropy, can be described and visualized. In Section 3 we focus on the electronic structure and magnetic anisotropy design that must be adopted to target specific functional materials. Each subsection of Section 3 contains a brief introduction describing the potential of the examined material, with the minimum number of equations necessary to introduce the relevant physical properties, and some outstanding examples. Importantly, the chemical guidelines provided here are mandatory but not always sufficient to achieve an optimal performance of a specific type of material. If this is the case, appropriate references addressing the remaining challenges are acknowledged.

2. Electronic structure and magnetic anisotropy

The electronic structure of a metal ion can be described using a Hamiltonian formalism in the framework of the Crystal Field theory. Although not exact, this description has the advantage of proving a tight

* Corresponding author.
E-mail address: mauro.perfetti@unifi.it (M. Perfetti).

https://doi.org/10.1016/j.ccr.2023.215213
Received 18 March 2023; Accepted 2 May 2023
Available online 15 May 2023

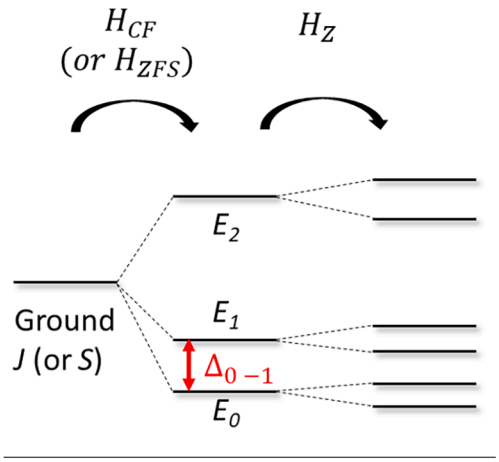

Fig. 1. Influence of the Crystal Field and of the Zeeman terms on the ground J (or S) multiplet. The red double arrow marks the separation between the ground and first excited state ($\Delta_{0\text{-}1}$).

connection with the chemical structure of the molecule. The effective Hamiltonian contains several terms:

$$\mathscr{H} = \mathscr{H}_0 + \mathscr{H}_{ee} + \mathscr{H}_{SO} + \mathscr{H}_{CF} + \mathscr{H}_Z \quad (1)$$

$\mathscr{H}_0$ represents the energy in the central field approximation and accounts for the kinetic and potential energy of the electrons in the electric field generated by the nuclei. $\mathscr{H}_{ee}$ describes the interelectronic repulsion. $\mathscr{H}_{SO}$ accounts for the Spin-Orbit coupling. $\mathscr{H}_{CF}$ describes the Crystal Field generated by the ligands. $\mathscr{H}_Z$, the Zeeman term, accounts for the effect of a magnetic field on the energy levels. Other terms, such as the hyperfine interaction, might be added to equation (1) but will not be discussed here.

For lanthanoids, the $\mathscr{H}_{SO}$ term dominates over the $\mathscr{H}_{CF}$ term due to the compact character of the partially filled 4*f* orbitals, therefore we consider the total spin (S) as tightly coupled with its orbital angular momentum (L) forming non-degenerate Russell Saunders multiplets described by a total angular momentum (J). The J multiplets can further split upon the action of the Crystal Field imposed by the ligands depending on the value of their projection along the z axis, *i.e.* m_J. The Crystal Field is generally described, for these systems, using Stevens operator equivalents, that are based on spherical harmonics [12,13].

$$\mathscr{H}_{CF} = \sum_{k=2,4,6} \sum_{q=-k}^{k} b_k^q \hat{\boldsymbol{O}}_k^q \quad (2)$$

Where b_k^q and $\boldsymbol{O}_k^q$ are the parameter and the operator, respectively, associated with the spherical harmonics of degree k and order q.

For light transition metals the large radial extent of the 3*d* orbitals causes significant covalency and therefore constrains the electrons in the electrostatic potential produced by the ligands. The orbital angular momentum is (partially) quenched and the resultant energy level structure relevant for the discussion of the magnetic properties can be, in most cases, satisfactorily described using a Spin Hamiltonian, *i.e.* an Hamiltonian acting on the basis of the total spin S. The effect of the ligands on the energy structure of these systems is modelled with the so-called Zero Field Splitting term of the Spin Hamiltonian:

$$\mathscr{H}_{ZFS} = D\left(\hat{S}_z - \frac{1}{3}\hat{S}^2\right) + E\left(\hat{S}_x^2 - \hat{S}_y^2\right) \quad (3)$$

where D and E are the axial and rhombic Zero Field Splitting parameter, respectively. Of course, it must be kept in mind that this approximation has its own limitations, described elsewhere [14]. The residual orbital angular momentum of light transition metals is usually accounted for in the Zeeman term:

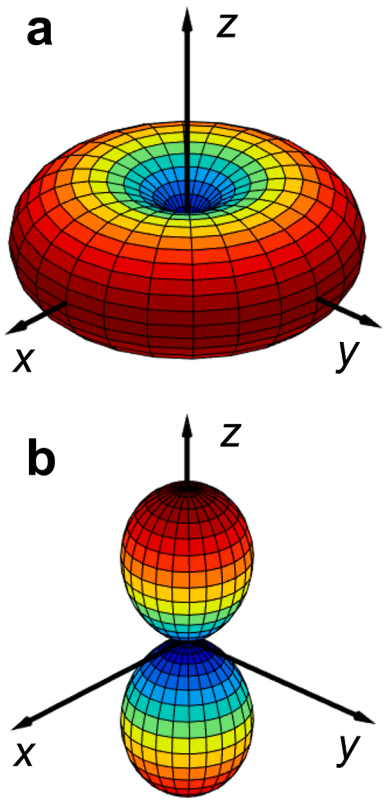

Fig. 2. Most common magnetic anisotropy shapes derived from the free energy. a) easy axis magnetic anisotropy. The z direction corresponds to a minimum in the free energy, *i.e.* an axis that can be easily magnetized. b) easy plane magnetic anisotropy. The xy plane corresponds to a minimum in the free energy, *i.e.* a plane that can be easily magnetized.

$$\mathscr{H}_Z = \mu_B \hat{\boldsymbol{S}} \bar{\bar{g}} \boldsymbol{B} \quad (4)$$

where the g tensor that couples the spin with the magnetic field is anisotropic. The anisotropy of g is the only source of magnetic anisotropy in $S = 1/2$ systems.

In Fig. 1 we have depicted the influence of the Crystal Field and of the Zeeman terms on the ground J (or S) multiplet. In this paper we propose to use the separation between the ground state and the first excited state ($\Delta_{0\text{-}1}$ in Fig. 1) as a good criterion to judge the potential of a molecule for a given application in the field of magnetic materials. The systems that we discuss in this review exhibit $\Delta_{0\text{-}1}$ values ranging from fractions of cm^{-1} to thousands of cm^{-1}. Therefore, the most suitable spectroscopic technique for the evaluation of $\Delta_{0\text{-}1}$ is system-dependent. A detailed explanation of the commonly used experimental setups in the detection of $\Delta_{0\text{-}1}$ is beyond the scope of the review, however we cite here some references that can be used to familiarize with such techniques. For materials with $10 < \Delta_{0\text{-}1} < 2000$ cm^{-1}, the energy level structure is typically measured using low temperature Luminescence [15–17], Inelastic Neutron Scattering [18] or In-Field Far Infrared Spectroscopy [17,19,20]. On the contrary, materials with $\Delta_{0\text{-}1} < 15$ cm^{-1} are conveniently measured using EPR spectroscopy at various fields and frequencies [21–23].

The type of magnetic anisotropy can also be important, and in the following paragraphs we will discuss why the magnetic anisotropy of some materials must be designed to have a certain shape. Magnetic anisotropy is usually classified as “easy axis” or “easy plane” (“easy cone” and other exotic magnetic anisotropy shapes are discussed elsewhere [4,24]). In general, the descriptor “easy” and “hard” denote an energetically favoured and unfavoured direction, respectively. The shape of magnetic anisotropy can be described using different physical

quantities: free energy, magnetization, or magnetic susceptibility.

The free energy F, in equilibrium conditions, can be defined as follows:

$$F(T, B(\theta,\varphi)) = -k_B T \ln Z = -k_B T \ln\left(\sum_{i=1}^{n} e^{-\frac{E_i(\boldsymbol{B}(\theta,\varphi))}{k_B T}}\right) \quad (5)$$

where k_B is the Boltzmann constant, T is the absolute temperature, $\boldsymbol{B}(\theta,\varphi)$ is the external applied magnetic field vector expressed in spherical coordinates, the summation runs over all the n states of the system and E_i is the energy of the i-th state.

The magnetization (M) can be retrieved by deriving the free energy with respect to the magnetic field:

$$\boldsymbol{M}(T, \boldsymbol{B}(\theta,\varphi)) = -\frac{\partial F(T, \boldsymbol{B}(\theta,\varphi))}{\partial \boldsymbol{B}(\theta,\varphi)} \quad (6)$$

The magnetic susceptibility (χ) can be obtained by further derivation:

$$\chi(T, B(\theta,\varphi)) = -\frac{\partial \boldsymbol{M}(T, \boldsymbol{B}(\theta,\varphi))}{\partial \boldsymbol{B}(\theta,\varphi)} = \frac{\partial^2 F(T, \boldsymbol{B}(\theta,\varphi))}{\partial (\boldsymbol{B}(\theta,\varphi))^2} \quad (7)$$

In most experimental conditions and for most compounds the description of the magnetic anisotropy based on the aforementioned three quantities coincides. However, this is not always the case [4]. Plots that ease the visualization of the free energy corresponding to the most common magnetic anisotropy landscapes are reported in Fig. 2. The free energy of an easy axis system appears as a "donut" in which the hole corresponds to the lowest energy direction (usually z), that is, the easy axis. The xy plane corresponds to the maximum free energy value and it is therefore called hard plane. Instead, the easy plane free energy plot resembles the $2p_z$ orbital. The nodal plane of the orbital (xy plane) corresponds to the minimum F direction and it is therefore called easy plane. The z axis of this plot corresponds to the maximum F, *i.e.* the hard axis. The plots describing the magnetic anisotropy of M and χ usually have opposite shape compared to the ones obtained from F [24].

It is finally important to remark that some compounds can have different types of magnetic anisotropy depending on external stimuli such as temperature, magnetic field, and pressure. We will discuss this class of materials in Section 3.5. For all the other materials described here, the targeted magnetic anisotropy is intended as the magnetic anisotropy that the material exhibits at the described (or desired) experimental conditions.

3. Molecular magnetic functional materials and their design

3.1. Single molecule magnets

Magnetic bistability of molecular origin in coordination compounds was discovered in 1993 [25]. A bistable magnetic molecule can be magnetized along a certain axis and retains its magnetization for a long time in absence of applied magnetic field. This peculiarity renders Single Molecule Magnets (SMM) extremely appealing for data storage at the molecular level. The foreseen possibility to use molecules as bits paves the way to miniaturize the storage devices by more than two orders of magnitude [26], effectively promoting a more efficient and considerate use of resources.

The basic working principle of SMM, as in classical bits, stems from a bistable ground state, that occurs if the magnetic anisotropy is of easy axis type. A pictorial way to represent the energy level scheme associated with a SMM is a double-well potential such as the one reported in Fig. 3. In this picture the two wells bottoms represent the opposite orientations of the magnetization (*i.e.* up and down). The application of a magnetic field removes the degeneracy of the ground state (favouring one orientation over the other) allowing the selective population of one well. When the field is removed, the spins remain "trapped" in the well for a characteristic period of time called relaxation time (τ). The temperature at which the value of τ reaches 100 s is called blocking temperature (T_B) and is related to the quality of a SMM (the higher the better).

The value of τ stems from the relaxation processes that contribute in reversing the orientation of the magnetic moment. A detailed description of all the relaxation processes, and their usual relative magnitude in molecules with different chemical composition is reported elsewhere [27–30]. Here we will just describe the three most important relaxation processes in high performance SMM called Quantum Tunnelling (QT), Orbach, and Raman.

The Raman relaxation is a two-phonon process and its dependence has not been trivially related to the electronic structure of the system. Seminal works of Chilton [31] and Lunghi [27,28] suggest that a careful engineering of the intramolecular (optical) and intermolecular (acoustic) phonons is key to achieve control over this process. On the contrary, Orbach and QT have a strong connection with the electronic structure and the magnetic anisotropy of the system. Eq. (8) shows the contribution to the temperature dependence of the relaxation time by the QT and Orbach processes (first and second term in Eq. (8), respectively):

$$\tau = \tau_{tun} + \tau_0 e^{U_{eff}/k_B T} \quad (8)$$

Where τ_{tun} is the tunnelling time, τ_0 is the pre-exponential factor, U_{eff} is the barrier for the relaxation of the magnetization and $k_B T$ is the thermal energy.

QT is a very detrimental process that involves the tunnelling of the spin through the barrier. It is usually considered temperature-independent and it can be tuned by changing the applied field and/or varying the composition of the states involved in the transition (*e.g.* by appropriate tuning of the Crystal Field) [32–34]. More specifically, it has been theoretically predicted [35] and experimentally demonstrated [34] that a high purity of the ground state (*i.e.* low mixing) minimizes the influence of QT in the slow relaxation. Recent works suggest that coupling with phonons could also contribute in mixing the levels and therefore modifying QT [36–38].

The Orbach process requires to absorb resonant phonon(s). Sometimes (especially in lanthanoids-based SMM) the relaxation can occur via the absorption of a single resonant phonon and then QT. This process is called Thermally Assisted Quantum Tunnelling (TA-QT) and effectively decreases the U_{eff} (often to $\Delta_{0\text{-}1}$). A representation of these two processes is reported in Fig. 3. Independently from the preferred

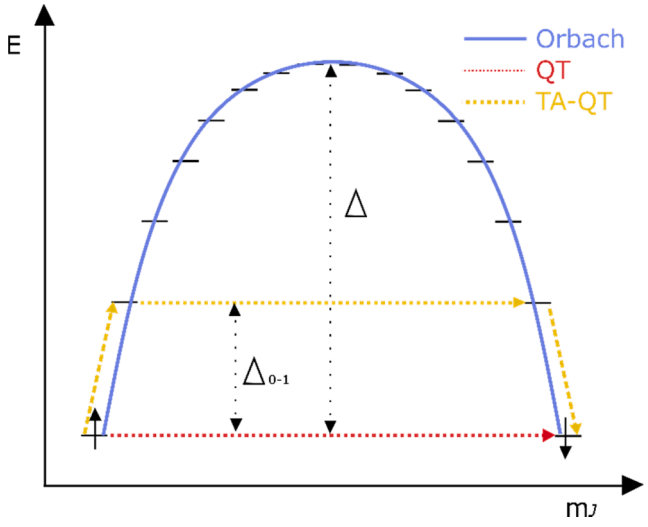

Fig. 3. Double well potential of a SMM and most relevant relaxation processes. The red and the yellow arrows represents Quantum Tunnelling and Thermally Assisted Quantum Tunnelling, respectively, the blue line represent the Orbach relaxation process.

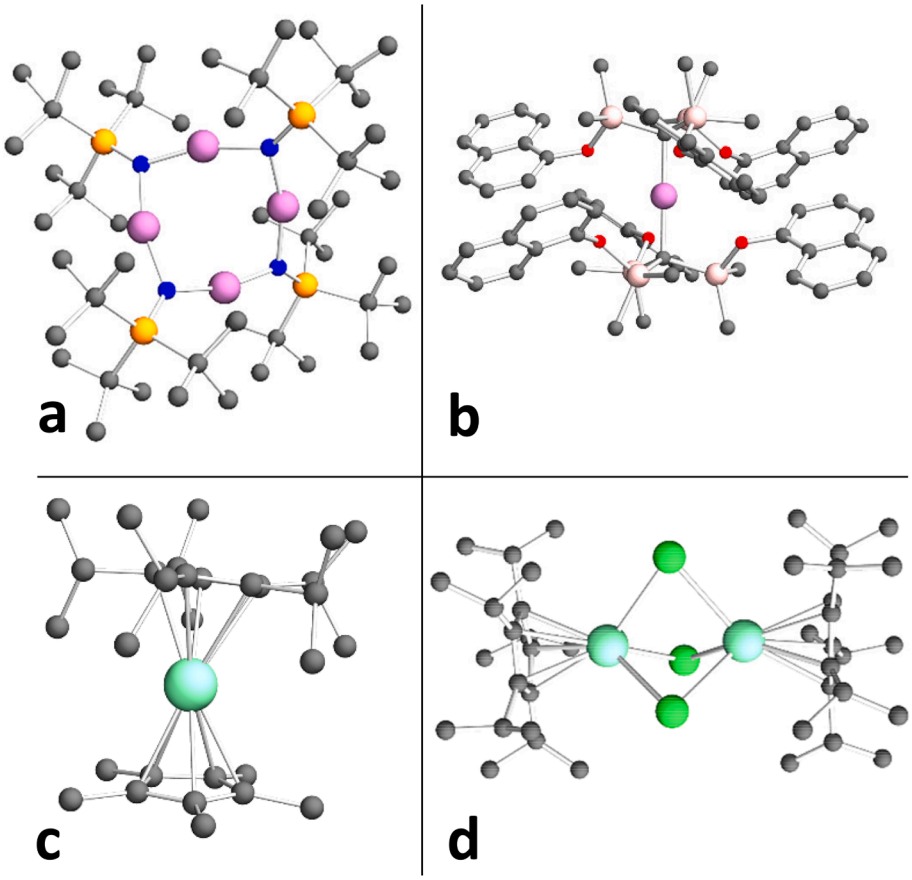

Fig. 4. Current best performant SMM of different nuclearity and chemical composition. a) Polynuclear transition metal: $[Co_4(\mu\text{-}NP^tBu_3)_4]^+$ [43] b) Mononuclear transition metal: $[Co(C(SiMe_2ONaph)_3)_2]$ [19] c) Mononuclear lanthanoid: $[(Cp^{iPr5})DyCp^*]^+$ [84] d) Polynuclear lanthanoid: $[(Cp^{iPr5})_2Dy_2I_3]$ [90]. Colour code: Co: purple, Dy: aquamarine, N: blue, O: red, P: orange, C: grey, Si: light pink, I: green. H atoms were omitted for clarity.

thermally active relaxation pathway (either Orbach or TA-QT), the target $\Delta_{0\text{-}1}$ value must be as large as possible to increase the working temperature of a SMM. Therefore, the most relevant candidates as high performance SMM are molecules possessing a large $\Delta_{0\text{-}1}$ and easy axis magnetic anisotropy.

In order to target this specific type of electronic structure and magnetic anisotropy, the chemical design of the molecule depends on the chosen metal ion [5,39–41]. As discussed in Section 1, in complexes containing first row transition metals the ligand's repulsion dominates over the SOC. This produces highly symmetric molecules allowing to deduce the magnetic anisotropy, in many cases, by simple geometric considerations. However, the quenching of the orbital angular momentum reduces the magnetic anisotropy. Nonetheless, the first SMM were based on transition metal clusters to achieve very high values of the total spin [42]. The Co_4 cluster reported by the Long group (Fig. 4a) holds, to the best of our knowledge, the record barrier $U_{eff} = 87\ cm^{-1}$ ($B = 0.1$ T) and $T_B = 3.6$ K (butterfly hysteresis) [43]. Another remarkable example is the Mn_6 cluster reported by Brechin et al., that has a lower barrier ($U_{eff} = 62\ cm^{-1}$) but in zero applied field, and a classical hysteretic behaviour with $T_B = 3.5$ K [44]. Although this research line has produced an essential understanding of the physics of mesoscopic systems [45–47], the barriers of these molecules remained relatively modest. In 2007, a seminal paper by Waldmann pointed out that the height of the anisotropy barrier in these systems increases as S^0 and not as S^2, as naively expected from Eq. (3) [48].

Targeting molecules containing ions with large orbital contribution is much more appealing. A literature review clearly shows that trigonal bipyramidal Ni^{2+} [49] or tetrahedral Co^{2+} complexes [50,51] are good SMM. However, linear complexes with weak donor ligands are the most rewarding [19,52–54]. because the linear coordination prevents Jahn Teller distortion, therefore maintaining a doubly degenerate ground state (d_{xy} and d_{xy}^2 orbitals) and the high symmetry avoids level mixing effectively reducing QT [32]. At the same time, the weak ligand field assures a high spin configuration and favours a Hund's rule arrangement of the spins (maximization of the orbital angular momentum) instead of the common lowest energy orbital filling. To the best of our knowledge, the record barrier for the reversal of the magnetization has been reported in 2018 by Long and co-workers on $[Co(C(SiMe_2ONaph)_3)_2]$, see Fig. 4b [19]. This molecule has indeed retained the largest orbital angular momentum achievable for transition metal ($L = 3$) and exhibits the largest spin compatible with it ($S = 3/2$). The low ligand field strength allows the insurgence of a total angular momentum $J = 9/2$, with an impressive barrier of $450\ cm^{-1}$.

The alternative to achieve very high orbital angular momentum in the ground state is the use of lanthanoids, where SOC is dominant [55]. The relatively high atomic number of lanthanoids and low radial extension of the partially filled *4f* orbitals is well suited to avoid orbital quenching, therefore providing a source of magnetic anisotropy in connection with appropriate Crystal Field design. Indeed, a golden rule has been extracted: strong easy axis magnetic anisotropy can be achieved by coordinating ions with prolate electron density of its highest m_J state (*e.g.* Er^{3+}) with an equatorial ligand or ions with oblate electron density of its highest m_J state (*e.g.* Dy^{3+}) with an axial ligand [56,57]. However, the low Crystal Field potential compared to the SOC, and the large ionic radius, pose experimental difficulties in controlling the coordination geometry of lanthanoid complexes. This problem has been recently tackled in several ways. Planar O-based or N-based neutral ligands have been used to lock the equatorial positions and leave space to axial charged

ligands in complexes of oblate ions such as Ho^{3+} [58] and Dy^{3+} [59–68]. Alternatively, bulky equatorial ligands have been used to exclude axial coordination in Er^{3+}-based SMM [69]. It is worth noticing that several axially coordinated Er^{3+}-based organometallic complexes have also been reported [70–73]. Also inserting lanthanoid in fullerene cages provides an axial Crystal Field with remarkable magnetic properties [74–76]. However, the most successful strategy so far has been the use of rigid and densely charged organic cyclic ligands [77–83]. The current record was obtained by Layfield and co-workers for $[(Cp^{iPr5})DyCp^*][B(C_6F_5)_4]$ (Cp^{iPr5} = penta-*iso*-propylcyclopentadienyl, Cp* = pentamethylcycl opentadienyl). This complex, reported in Fig. 4c, has a barrier of 1541 cm^{-1} and a blocking temperature of 65 K [84]. It is worth mentioning that very recently the complex $[K(18\text{-crown-6})][Dy(BC_4Ph_5)_2]$ with comparable blocking temperature and barrier (65 K and 1500 cm^{-1}, respectively) has been reported [85].

Due to the unquenched orbital momentum, the possibility to strongly couple several lanthanoids could seem appealing [86]. However, the very same reason why lanthanoid-based mononuclear SMM are performant, *i.e.* the compact nature of the *4f* orbitals, constitutes an obstacle for promoting efficient magnetic exchange between centres. In the last decade, the synthesized polynuclear *4f*-based SMM have shown moderate potential [87–89]. The game-changer in this context was reported by Long and co-workers in 2022. The molecule $[(Cp^{iPr5})_2Dy_2I_3]$ (Fig. 4d) contains two lanthanoids of mixed valence (Ln^{2+}/Ln^{3+}) and a *d* electron equally shared between the two centres. This valence delocalization is key to impart a parallel alignment of the spins, which in turn generates a barrier of 1631 cm^{-1} and a blocking temperature of 72 K [90].

It is worth mentioning that coupling *4f* metals with diffuse radicals can enhance the magnetic properties [91–95] leading to remarkably large hysteresis loops [96–101].

Finally, actinoids might seem a perfect building block for SMM due to the relatively large radial extension of the *5f* orbitals and the unquenched orbital angular momentum. However, the best performances obtained so far with these ions are modest [102–105] and the strategy of synthesizing multinuclear systems seems the most rewarding [106,107].

3.2. Pseudo contact shift agents

Nuclear Magnetic Resonance (NMR) is an extremely useful tool to determine the structure of molecules. However, in very large molecules (*e.g.* proteins) many NMR signals could fall in a relatively narrow range, crowding the spectrum and making peak assignment difficult. A local magnetic field can shift the nearby signals depending on the relative orientation between the field and the nuclei. Since the electron magnetic moment is 660 times greater than the proton one, unpaired electrons can be used to produce intense local fields.

A Pseudo Contact Shift agent (PCS) is a paramagnetic molecule able to shift the NMR signals of the nuclei placed in its proximity [108,109]. Discovered in 1996 [110], they have been successfully used for the structural determination of biomolecules [111–114], even in-cell [115].

The pseudo contact shift depends only on the anisotropic character of the magnetic susceptibility [116]. In a reference frame where the susceptibility tensor is diagonal, the pseudo contact shift assumes the following form:

$$\delta^{pc} = \frac{1}{12\pi r^3}\left[\Delta\chi_{ax}\left(3\cos^2\theta - 1\right) + \frac{3}{2}\Delta\chi_{rh}\sin^2\theta\cos 2\varphi\right] \quad (9)$$

where r, θ and φ are the spherical coordinates defining the position of the nucleus with respect to the paramagnetic centre, and

$$\Delta\chi_{ax} = \chi_{zz} - \frac{\chi_{xx} + \chi_{yy}}{2} \quad (10)$$

$$\Delta\chi_{rh} = \chi_{xx} - \chi_{yy} \quad (11)$$

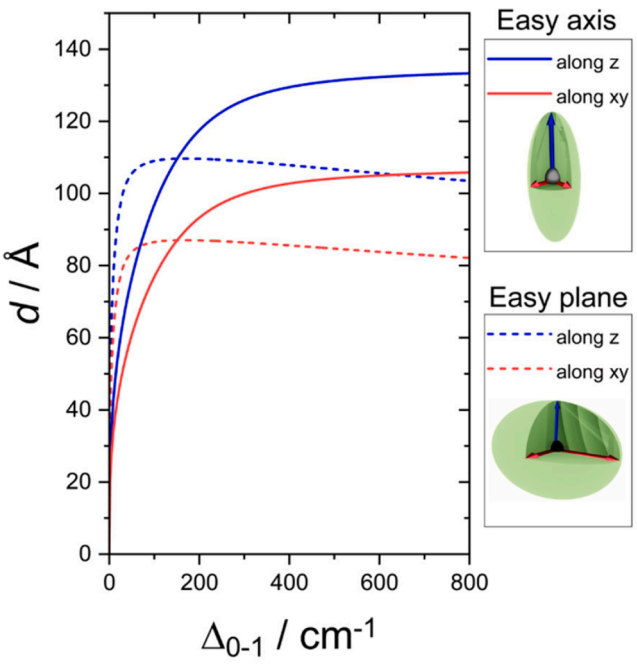

Fig. 5. Distance from a Dy^{3+} ion with easy axis magnetic anisotropy (solid lines) and easy plane magnetic anisotropy (dashed lines) at which a shift of | 0.05| ppm is observed. The blue and red curves represent shifts of nuclei along the *z* axis and the *xy* plane, respectively. The green ellipsoids represent the magnetic susceptibility.

Here χ_{xx}, χ_{yy}, χ_{zz}, are the principal components of the susceptibility tensor, therefore $\Delta\chi_{ax}$ defines the axiality (*i.e.* how much the susceptibility along *z* differs from the average susceptibility in the plane) and $\Delta\chi_{rh}$ defines the rhombicity (*i.e.* the anisotropy in the *xy* plane). A detailed discussion on the relaxation time and magnetic anisotropy influence on, *e.g.*, the signal broadening is outside the scope of this review. However, we must mention that long relaxation times and high magnetic anisotropy cause significant signal broadening, therefore reaching a reasonable compromise between high anisotropy and signal broadening is often crucial, as reviewed in literature [108].

The influence of magnetic anisotropy is, in PCS literature, conveniently discussed using the anisotropy of the magnetic susceptibility ($\Delta\chi$) as descriptor because $\Delta\chi$ is directly proportional to the obtained shift (Eq. (9)). Since magnetic anisotropy stems from spin orbit coupling, the same metal ions used in the design of SMM are the most common in PCS [117,118]. Indeed, in the last 10 years the field was dominated by the use of lanthanoid complexes, and, to a lower extent, Co^{2+} high spin (S = 3/2) and Fe^{3+} low spin (S = 1/2) complexes [108,109]. Room temperature typical values of $\Delta\chi_{ax}$ are of the order of 10^{-31} (heavy lanthanoids) or 10^{-32} m^3 (light lanthanoids and transition metals). Since most biomolecules maintain their structure only at very stringent pH and temperature conditions, the structure, stability and solubility of the complexes become key factors. Indeed, the majority of the ligands recently studied for PCS purposes are polydentate ligands such as cage ligands [119–121] or functionalized macrocyclic cavities [109,122,123].

Keeping $\Delta\chi_{ax}$ constant and changing its sign (*e.g.* from easy axis to easy plane) has no effect on the magnitude of the induced pseudo contact shift, as evident from equation (9). For example, $[TmDOTA{\cdot}H_2O]^-$ and $[DyDOTA{\cdot}H_2O]^-$ (DOTA = 1,4,7,10-tetraazacyclododecane N,N', N'',N'''-tetraacetate) possess comparable $\Delta\chi_{ax}$ (positive and negative respectively, at room temperature) [124,125] and they indeed produce similar shifts [108].

However, from a practical point of view the most immediate strategy to increase the magnetic anisotropy is maximizing $\Delta_{0\text{-}1}$, as discussed for

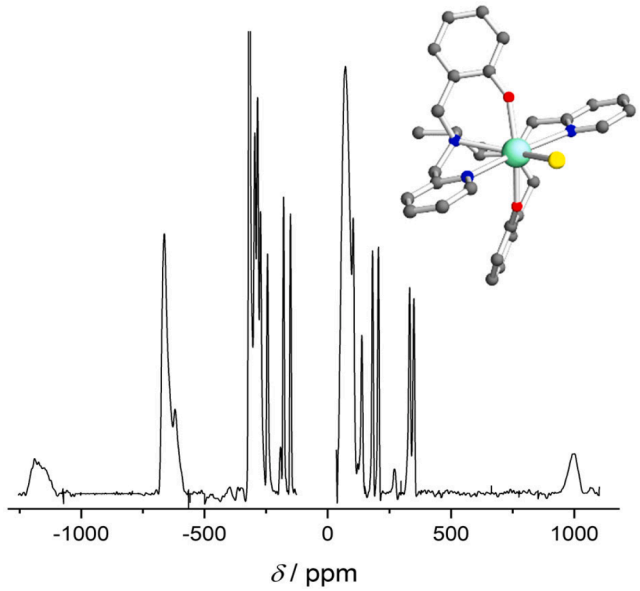

Fig. 6. Experimental ^{1}H NMR spectrum, and structure of Dy(bbppn)Cl [118]. The spectrum was recorded at 293 K and 9.4 T in CD_2Cl_2. Colour code: Dy: aquamarine, Cl: yellow, O: red, N: blue, C:grey. H atoms omitted for clarity.

SMM. In Fig. 5 we have reported the distance at which a shift of |0.05| ppm can be observed at $T = 300$ K and $B = 15$ T for a perfectly easy axis (straight lines) and easy plane (dashed lines) Dy^{3+} ion ($J = 15/2$ and $g_J = 4/3$) as a function of $\Delta_{0\text{-}1}$. The shape of the curves depend on the magnetic anisotropy of the system. For an easy axis system, enlarging $\Delta_{0\text{-}1}$ increases the magnetic anisotropy, effectively allowing to observe the shifts at longer distance, and the curves tend to saturate when the ground state is the only one significantly populated. For easy plane systems, the curves show a peak after which the magnetic anisotropy decreases and so does the pseudo contact shift. This phenomenon is due to the decrease of the magnetic moment that an easy plane system experiences when only the ground state gets populated and it is in fact particularly relevant for non-Kramers ions (ground $m_J = 0$ for axial easy plane systems).

By comparing the curves in Fig. 5 along, *e.g.*, the *z* axis, it is possible to extract the best magnetic anisotropy to target when the purpose of the experiment is mapping the largest portion of space. It is evident that easy axis systems with sufficiently large $\Delta_{0\text{-}1}$ can shift signals at longer distance than easy plane systems. In other words, with a fixed $\Delta_{0\text{-}1}$ an easy axis system is more anisotropic than the corresponding easy plane one. Although the exact value of $\Delta_{0\text{-}1}$ at which the magnetic anisotropy of an easy plane and an easy axis system equate depends on the considered ion, the conclusion that easy axis magnetic anisotropy must be preferred over easy plane is general. This is a positive news for Chemists, because lanthanoid ions with large total angular momentum values are more prone to exhibit an easy axis magnetic anisotropy than an easy plane one, as theoretically predicted [35] and experimentally demonstrated [125]. Following this simple reasoning, Sessoli and co-workers recently exploited the same magnetic anisotropy design employed for SMM to engineer a promising PCS [118]. The structure of the molecule, Dy(bbppn)Cl (H_2bbppn = N,N'-bis(2-hydroxybenzyl)-N,N'-bis(2-methylpyridyl)-1,2-propylenediamine), is reported in Fig. 6 and a thorough magnetic study revealed an extremely pronounced easy axis anisotropy at all temperatures and fields. At the conditions of the NMR experiment (293 K and 9.4 T) the shifts produced on the ligand protons exceed 1000 ppm, as reported in Fig. 6. The value of $\Delta\chi_{ax}$ and $\Delta\chi_{rh}$ are 2.16 10^{-30} m^3 and −2.17 10^{-32} m^3, respectively. Such a high axiality has the potential to produce shifts of 0.05 ppm at a distance as high as 130 Å (along the *z* axis of the molecule). This value, to the best of our knowledge, outperforms all current PCS and demonstrates that SMM and PCS can be designed with similar principles.

It is now interesting to comment on how to map crowded environments, a very common scenario in biological systems. Let's suppose to have a sphere of protons at, *e.g.*, 5 nm from the paramagnetic centre. The acquisition of the NMR spectrum using an hypothetical PCS axial system with $\Delta\chi_{ax} = 10^{-30}$ m^3 would reveal shifts of ~ 400 ppm along the *z* axis and of −200 ppm in the *xy* plane, therefore not allowing an unambiguous mapping of the *xy* plane. This problem has been elegantly tackled using chemistry. Changing the length of the chemical linker connecting the PCS to the protein allows to access different spatial conformations, providing complementary information [126]. In the case of quite rigid linkers, also rhombicity can be considered as a useful asset to impart different shifts to the ^{1}H nuclei in the *xy* plane. For instance, maximizing the rhombicity of the aforementioned tag would impart chemical shifts of −320 and −107 ppm to protons along the *y* and *x* axis, respectively, therefore boosting the spatial resolution in the *xy* plane.

3.3. Optically Addressable Qubits

Quantum bits, or qubits (QB), are quantum objects that can be prepared in a coherent superposition state, $\psi = \alpha|0\rangle + \beta|1\rangle$ [127]. This characteristic renders them somewhat complementary to SMM: while SMM are two-states systems, and are therefore suitable for classical information storage, QB are much more appealing for processing and transmitting coherent quantum information. QB have the potential to be game-changers in several fields. For example, thanks to the no-cloning theorem (*i.e.* the impossibility to prepare an independent and identical copy of an arbitrary unknown quantum state [128]) QB could revolutionize the field of cryptography. Another intriguing perspective is the possibility to simulate the properties of matter using bits that obey the same laws as atoms (*i.e.* quantum mechanics). A fascinating and realistic perspective on the future quantum internet [129,130] was recently reported by Laorenza and Freedman [131].

In 2000, DiVincenzo distilled the five essential characteristics that a QB must possess [132]: I. A QB must be well-defined and scalable to produce QB architectures, II. It must have the proper electronic structure to be initialized in a defined state, III. It must possess an appropriate coherence time (*i.e.* the lifetime of the superposition state) to perform operations, IV. It must be able to perform a set of quantum operations, V. It must be individually measurable.

At the present stage, the prime candidates to realise quantum networks are solid state defects in materials [133,134], or superconducting circuits [135–137]. For example, nitrogen vacancies have shown potential for quantum teleportation of an arbitrary quantum superposition state with average state fidelity exceeding the classical limit [138]. However, the advantages of molecular spins are rapidly putting molecules back in the race [139–141]. Molecular QB are not bound to a specific host and they can be arranged in architectures of various dimensionality [127,142,143], therefore satisfying the first DiVincenzo criterion. Moreover, their properties can be finely tuned by the judicious use of coordination chemistry [144–149].

To demonstrate that the electron spin can be coherently controlled, a pulsed EPR experiment is usually performed, and the Rabi oscillations typical of a two-levels quantum system are extracted [150]. In practical terms, the manipulation of a QB requires that the two involved states can be coupled by readily available microwave frequencies in an EPR experiment. Therefore, the simplest QB that can be imagined is an $S = 1/2$ molecule. Many such molecules have been synthetized and proposed as possible QB [140]. A chemical approach has been used to pinpoint the main sources of decoherence, that are the fluctuating fields caused by the nuclear spins > 6 Å away from the spin centre [151,152]. This problem can be circumvented by the usage of elements with null nuclear spin or specific isotopes [153–155], or by the exploiting transitions less sensitive to the environment such as clock transitions [139,156,157]. However, the first approach has an obvious economical drawback and can be seldomly applied in organic chemistry, while the second partially

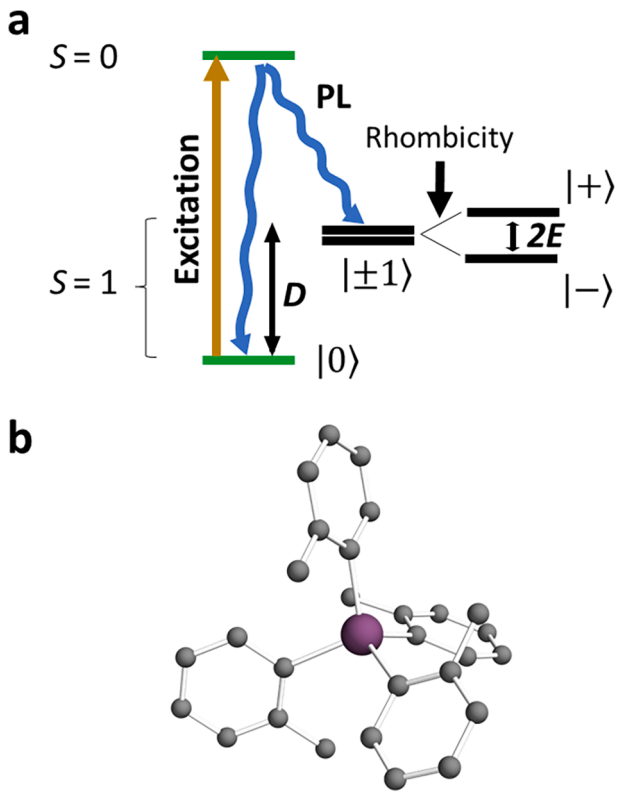

Fig. 7. a) Energy level scheme and initialization process for an $S = 1$ molecular QB. The symbols $|+\rangle$ and $|-\rangle$ represent the linear and antilinear combination of the $|m_s\rangle = |\pm1\rangle$ states belonging to the ground $S = 1$ multiplet. b) Structure of Cr(o-tolyl)$_4$ [165]. Colour code: Cr: violet, C: grey, H omitted for clarity.

nullify the tuneability advantage and the possibility to couple molecular QB [127].

With these premises, it might seem that an electronic structure design is superfluous for QB. Indeed the only initialization process possible for such a system is a thermally-driven one, *i.e.* applying a magnetic field and lowering the temperature enough to selectively populate the ground state. At fields of the order of 1 T, a selective population of the ground state (>99%) can be achieved at $T < 290$ mK, making $S = 1/2$ QB suboptimal to satisfy the second DiVincenzo criterion.

This problem can be overcome by optical initialization using the ZFS of, *e.g.*, $S = 1$ systems. Indeed, the initialization mechanism of nitrogen vacancies in diamond [158], divacancies in silicon carbide [159] and chromium impurities in gallium nitride [160] occurs exploiting the electronic structure of the $S = 1$ "impurity". In 2018 Freedman and co-workers proposed to mimic this initialization process in molecular qubits, labelling this type of materials Optically Addressable Qubits (OAQB) [161]. In order to synthesize OAQB candidates several criteria must be met. First of all, a state $m_S = 0$ must be present in the ground multiplet, therefore non-Kramers ions must be selected. Among these, ions with $S = 1$ must be preferred in order to minimize the number of involved states. Moreover, the value of $\Delta_{0\text{-}1}$ must be commensurate to the EPR microwave energy (0.3 cm^{-1} in the X-band spectrometers) to allow manipulation. The rest of the electronic structure (*i.e.* the first excited spin multiplets) must also be carefully engineered via a combination of (strong) ligand field and (high) molecular symmetry to allow appropriate optical control. A more thorough guideline to address this point can be found in the literature [161], while here we simply describe the electronic structure and initialization process recently proposed by Awshalom and Freedman on a series of Cr^{4+} complexes [162].

Although simplified, the scheme reported in Fig. 7a captures the physics of the process. A resonant optical pulse excites the spins from the $|0\rangle$ ("bright") state belonging to the ground $S = 1$ state to an excited $S = 0$ state. Then, spontaneous photoluminescence occurs and the spins can either relax to the $|0\rangle$ state (and then getting re-excited) or to the $|\pm1\rangle$ ("dark") states. If the characteristic relaxation time of the spins in the ground state (T_1) is longer than the excited state lifetime (T_{opt}), multiple cycles accumulate polarization in the $|\pm1\rangle$ states (*i.e.* allow initialization). The optical contrast between the start and the end of a single pulse effectively constitutes a lower limit on the spin polarization. Notably, if the transition between the ground and excited state is sufficiently narrow, both initialization and readout can be performed. Since the polarization process occurs due to the composition of the states (and not their relative energy), the sign of the ZFS parameter is immaterial for this application. Great progress in this area has been done over the last few years with V^{3+} [163], Ni^{2+} [164], and Cr^{4+} [165] complexes.

It is now intriguing to discuss the role of the rhombicity in this

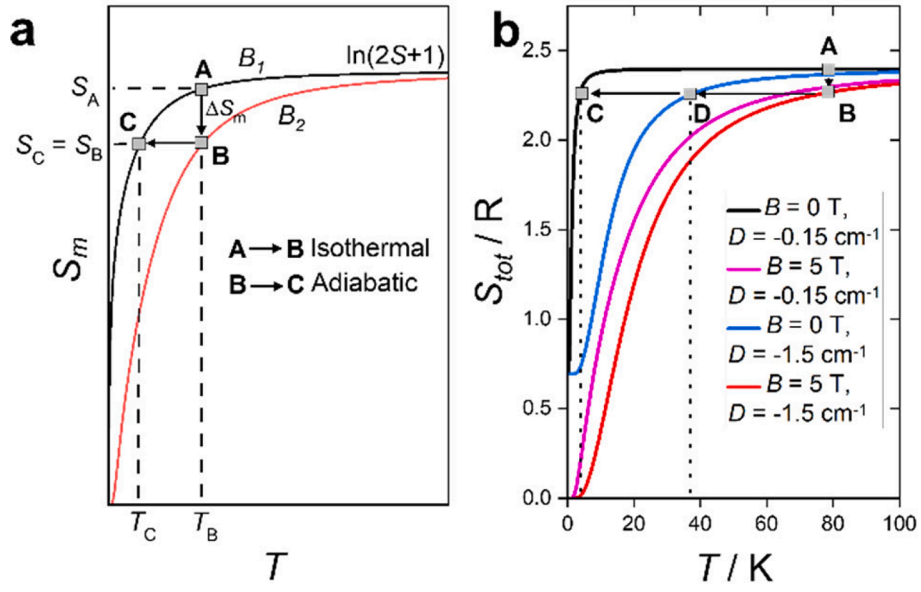

Fig. 8. a) Simplified mechanism describing the magnetocaloric effect. b) Influence of the ZFS parameter on the magnetocaloric effect.

process. If rhombicity is null (*i.e.* the $|+1\rangle$ and $|-1\rangle$ states are degenerate) the complex is, in zero field, a simple two level system. This is the case of Cr(*o*-tolyl)$_4$ (Fig. 7b) [162]. However, if the complex has some degree of rhombicity the degeneracy of the doublet is removed and the two states become the linear and antilinear combination of $|\pm1\rangle$ ($|+\rangle$ and $|-\rangle$ in Fig. 7a). This degeneracy removal constitutes an asset because the transition between these states is poorly sensitive to external perturbations (as in nuclear clock transitions) while maintaining the advantages of involving electron spins instead of nuclear spins. Rhombicity has been introduced by proper structural modification [162] or by dilution in a non-isostructural, lower symmetry matrix [166].

3.4. Magnetic Refrigerants

Many modern technologies require low temperatures to operate. In this article we have discussed two categories of materials (SMM and QB) that, at the present stage, require low temperature to work. However, there are many more, such as superconductors. If the desired operational temperature is below liquid nitrogen boiling temperature (77 K), liquid He is generally used. Nowadays cryogenics and superconductivity applications consume almost 30% of the global He supply [167]. However the price of this cooling fluid is rapidly raising due to the limited supply. Even more problematic is reaching very low temperatures because it usually requires ^{3}He, prohibitively expensive even compared to ^{4}He [168]. Nonetheless, 25 mK is the operational temperature of the most powerful quantum computers currently in use, therefore cryorefrigeration is a very active research field.

Molecular materials, thanks to their monodispersity and controllability, can offer a cheap and environmentally friendly solution to this problem by employing the Magneto Caloric Effect (MCE). Normal MCE is a physical process that exploits a change in magnetic entropy of a system upon application/removal of a magnetic field to cool the surroundings. Also the opposite effect, called reverse MCE, can be obtained and used for energy recovery [169], but we will not discuss it here. In conventional normal MCE setups the magnetic field is applied on a fixed single crystal or thin layer of molecules.

The molar magnetic entropy (S_m) of an isolated system can be obtained by simple derivation of the free energy with respect to the temperature [170]:

$$S_m(T,H) = -\left(\frac{\partial F}{\partial T}\right)_B = RT\left(\frac{\partial \ln Z}{\partial T}\right)_B + R\ln Z \quad (12)$$

where the symbols have the same meaning as in Eq. (5). If the system is paramagnetic, the levels in the partition function will correspond to different (combinations of) m_S or m_J.

Let's refer to Fig. 8a and consider a magnetic refrigerant in a condition A, with an associated entropy S_A, at temperature T_A and magnetic field B_1 (typically, $B_1 = 0$ T). If we increase the field to a value B_2, we expect a lowering of the entropy of the magnetic system due to the selective population of the lowest state(s), associated with heat release to the bath. If this process is conducted isothermally (*i.e.* the released heat is efficiently captured by heat sinks) we end up in the situation described by the point B in Fig. 8a. If we now perform an adiabatic demagnetization process (*i.e.* we lower the field to the previous value keeping the total entropy constant) the entropy that the magnetic system gains must be taken from the environment, with a consequent cooling (*i.e.* $\Delta T = T_C - T_B$, point C in Fig. 8a). Several types of refrigeration cycles based on this effect have been proposed [171].

For the purpose of this review it is now interesting to evaluate the role of the anisotropy in this process, while a rigorous treatment of the effect, that takes into account also the lattice entropy, is described in the literature [171–175]. We have plotted the zero field entropy vs temperature curves of two $S = 5$ systems with different ZFS values ($g = 2$ and $D = -0.15$ cm^{-1} or $D = -1.5$ cm^{-1}, black and blue curves in Fig. 8b, respectively). The black curve (referring to the system with the smaller ZFS) has a higher entropy at all temperatures. This can be simply explained by recalling that in the less anisotropic system more levels are thermally accessible. In the high temperature limit (all states equally populated in both systems) the entropy in zero magnetic field assumes the value $S_m = R \bullet \ln(\Omega) = R \bullet \ln(2S+1)$ (where S is the total spin). Since the entropy curves of these systems are almost identical at high

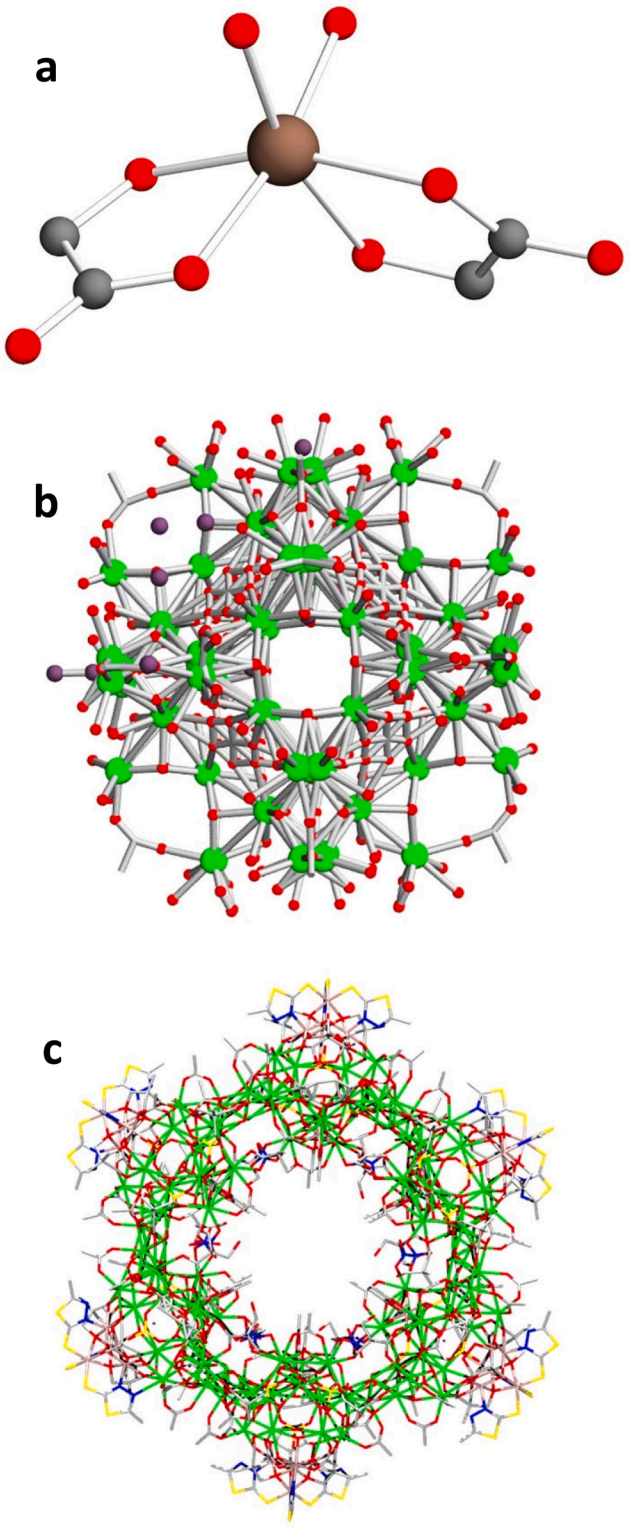

Fig. 9. Outstanding Molecular Refrigerants. a) Mn(glc)(H$_2$O)$_2$ [178] b) Gd$_{60}$ [189] c) Gd$_{102}$Ni$_{36}$ [191] Colour code: Mn: brown, O: red, Gd: green, Br: violet, C: grey, S: yellow, N: blue, Ni: light pink H atoms omitted for clarity.

temperature (*i.e.* the red and magenta curves are superimposable in the right region of Fig. 8b), the isothermal demagnetization process causes a larger temperature drop in the system with smaller magnetic anisotropy (*i.e.* $|T_C - T_B| > |T_D - T_B|$ in Fig. 8b). This result can be intuitively explained by recalling that magnetic anisotropy is necessary to provoke a thermal evolution of free energy in zero field (an isotropic system has a constant magnetic entropy), but the application/removal of the magnetic field must affect the partition function significantly to produce measurable temperature drops. In other words, the effect of a magnetic field variation on a very anisotropic system is negligible because the population of the states does not change significantly, and it is therefore not useful for conventional MCE purposes. The preferred sign of D in the literature is negative, because for certain positive values of D a reverse MCE can be observed [176]. Interestingly, a change in sign of the D parameter (*i.e.* a magnetic anisotropy change from easy plane to easy axis) has a lower impact on the curves than the same change in magnitude. For example, changing the sign of D from -0.15 cm^{-1} to $+0.15$ cm^{-1} enhances the MCE of only 4.2 % while the same relative change in magnitude (-0.15 cm^{-1} to -0.45 cm^{-1}) provokes a decrease of MCE of about 26 %. We can conclude that in these materials keeping the ZFS (and therefore Δ_{0-1}) sufficiently small has priority over designing the nature of magnetic anisotropy.

Although the most straightforward observable for evaluating the potential performance of a MCE agent is ΔT, this is not usually measured due to experimental difficulties in its detection. Instead, the preferred way to assess the potential of a MCE agent is to obtain other two quantities, namely the isothermal change in magnetic entropy (ΔS_m) and the cooling power or refrigerant capacity (RC) via magnetometric data. The former is simply defined as the difference between the entropy of the system in the field B_2 and the entropy of the system in the field B_1 (usually 0 T), and therefore corresponds to the isothermal process A-B in Fig. 8. Since the sign of ΔS_m is negative for normal MCE, literature usually reports its maximum absolute value. RC accounts for the effective amount of heat that is transferred between the hot and cold reservoirs [176,177].

Since the most desirable requirements extracted from our analysis are I. Large spin values and II. Small ZFS, the best metal ions to use in mononuclear complexes are the ones with half-filled configurations (total orbital angular momentum $L = 0$, since in these cases SOC only acts at the second-order to introduce magnetic anisotropy). Therefore Mn^{2+} and Gd^{3+} are ideal choices ($S = 5/2$ and $7/2$, respectively). This approach has indeed been used to produce impressive $|\Delta S_m|$ values. Currently, the record value for a mononuclear Mn^{2+} complex namely $Mn(glc)(H_2O)_2$ (glc = glycolate) is fixed at $|\Delta S_m| = 60.3$ J kg^{-1} K^{-1} ($B_2 = 7$ T) and has been reported by the group of Tong in 2014 (Fig. 9a) [178]. The reported value, scaled per mass, is even more impressive if one takes into account that the magnetic centres density in molecular materials is usually lower than in extended networks. The record value of $|\Delta S_m|$ for a mononuclear Gd^{3+} complex is held by [[Gd$(OAc)_3(H_2O)_2]_2]\cdot 4H_2O$ ($|\Delta S_m| = 40$ J kg^{-1} K^{-1} ($B_2 = 7$ T)) and has been reported by Evangelisti and co-workers [179]. However, many Gd^{3+} complexes have been reported and studied [180]. The key element that emerges from the analysis of the reported structures is the density of the magnetic centres, which increases with the use of lighter ligands. A good example of this concept was provided by Evangelisti who reported the compound $[Gd(HCOO)_3]$ exhibiting an extremely high magnetic density per unit volume [181]. Using the same ligand, yet more recently, a complex of formula $[Gd(HCOO)(C_2O_4)]_n$ with $|\Delta S_m|$ of 32.7 J kg^{-1} K^{-1} ($B_2 = 2$ T) has been reported [182].

Bimetallic clusters have also been studied for MCE purposes. The most intuitive combination of metals to use is a transition metal coupled with Gd^{3+} [183]. Ideal *3d* metals are fairly isotropic species such as Mn^{2+}, Fe^{3+}, Cr^{3+}, and Cu^{2+}. A good example in this sense was reported in 2013 by Colacio *et al.* in which a ferromagnetic coupling is observed between Mn^{2+} and Gd^{3+} and a $|\Delta S_m|$ of 23.5 J kg^{-1} K^{-1} ($B_2 = 7$ T) [184]. Bimetallic species with Cu^{2+} [185], Cr^{3+} [186], Fe^{3+} [187], and Ni^{2+} [188] have also been reported. Of course, another viable strategy is assembling polynuclear clusters of strongly interacting ions, as evidenced by fairly recent works. If the interactions are mostly ferromagnetic, the spin ground state can reach very high values while maintaining a relatively low magnetic anisotropy. This strategy has proven particularly rewarding for Gd-based molecules. The molecular cluster reported in Fig. 9b contains 60 ferromagnetically coupled Gd^{3+} ions (total spin $S = 210$) and it holds, to the best of our knowledge, the record value of $|\Delta S_m| = 48$ J kg^{-1} K^{-1} ($B_2 = 7$ T) [189]. It is worth mentioning that another cluster formed by 12 weakly couple Gd^{3+} atoms has been recently synthesized and exhibits remarkable properties ($|\Delta S_m| = 46$ J kg^{-1} K^{-1}, $B_2 = 7$ T) [190]. Another impressive result of $|\Delta S_m| = 41$ J kg^{-1} K^{-1} ($B_2 = 7$ T) was recently obtained by synthesizing a gigantic mixed *3d-4f* cluster containing 36 Ni^{2+} ions and 102 Gd^{3+} ions (total spin $S = 393$, Fig. 9c) [191]. Spin frustration has also been exploited as a source of large cooling power [192]. Indeed, the competition between ferro- and antiferromagnetic interactions leads to highly degenerate ground states that enhance $|\Delta S_m|$ [193].

Finally, it is worth mentioning that in the last years an alternative setup that exploits high magnetic anisotropy for MCE purposes has been proposed [176]. If a single crystal contains (mostly) collinear anisotropic molecules (details about collinearity in crystals can be found in literature [194]), the molar entropy will also be anisotropic. Therefore, rotating the sample under a constant magnetic field changes the entropy effectively producing a cooling cycle [195–197]. Importantly, this setup saves a significant amount of time and resources because changing the magnetic field is the most time consuming and expensive part of the process [198].

3.5. Magnetic anisotropy switches

In the previous paragraphs we have emphasized how $\Delta_{0\text{-}1}$ and magnetic anisotropy represent a common ground to design several cutting edge materials. Therefore, obtaining materials with switchable magnetic anisotropy is of high technological interest. Although the magnetic anisotropy switch can occur due to interlevel crossings, especially in molecular clusters [199,200], in this paper we will focus on mononuclear complexes exhibiting this phenomenon due to their intrinsic electronic structure. This class of materials, called molecular Magnetic Anisotropy Switches (MAS) was discovered by Perfetti and coworkers in 2018 [201]. MAS can switch their magnetic anisotropy thanks to external stimuli such as temperature, magnetic field, and pressure [4,24].

To understand the chemical design that must be followed to obtain MAS materials we must first pinpoint the origin of the switch. In this article we will discuss the phenomenon qualitatively, while a numerical evaluation of the effect is reported in literature [201]. Let's consider a hypothetical Ce^{3+} ion ($J = 5/2$, $g_J = 6/7$) in an axial Crystal Field. For certain Crystal Field parameters we can imagine having the following composition of the m_J states: ground state $|\pm 1/2\rangle$ at energy E_g, first excited state $|\pm 5/2\rangle$ at energy E_1, second excited state $|\pm 3/2\rangle$ at energy E_2. For the sake of simplicity, and without any loss of generality, we can neglect the presence of the second excited state assuming that its energy is sufficiently high to avoid its population at all the considered temperatures ($E_2 \gg E_1$). The corresponding Zeeman diagram of such a system with a magnetic field along the *xy* plane and along *z* is reported in Fig. 10. If only the ground state is populated (*i.e.* at low temperature) the resulting anisotropy is easy plane because the slope of the pure $|\pm 1/2\rangle$ level (*i.e.* its *g* factor) is higher in the *xy* plane than along *z* (18/7 vs 30/7). However, the opposite is true for the $|\pm 5/2\rangle$ level (0 vs 30/7). Therefore, if we increase the population of the first excited state by increasing the temperature (Fig. 10b) the anisotropy must switch to easy axis. The resulting magnetic anisotropy phase diagram is reported in Fig. 10c. In this simple scenario no level crossings were involved, and the effect originated from a simple change of population difference between the states. Our example can be trivially extended to consider the

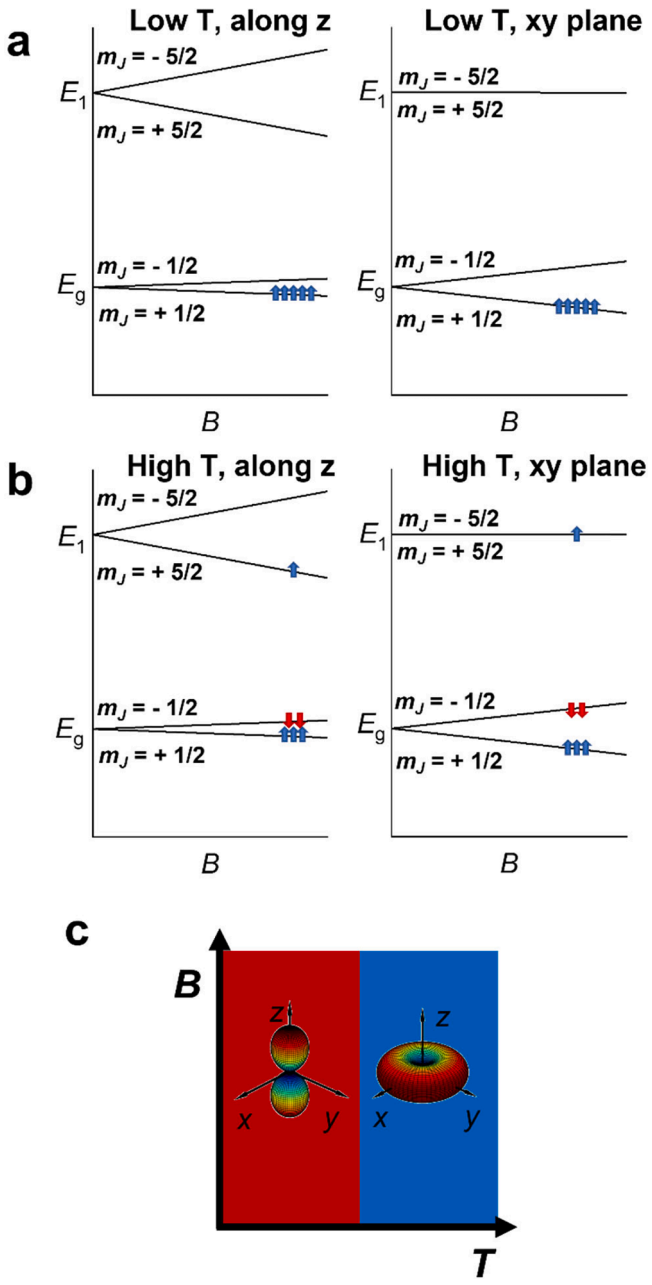

Fig. 10. a) Low and b) high temperature spin distribution of the levels of an hypothetical Ce^{3+} ion (see text for details). c) Resultant magnetic anisotropy phase diagram.

effect of a magnetic field or pressure change [24]. If more (possibly mixed) levels are involved, the picture gets more complicated but the physics of the effect described here remains valid [24,201]. For such reason, we will describe here a simple chemical recipe to obtain MAS based on ground and first excited state only.

The two key parameters to control for designing *ad hoc* molecular switches are, in close resemblance with the other materials described in this paper, $\Delta_{0\text{-}1}$ and the level composition. $\Delta_{0\text{-}1}$ must be kept sufficiently small to have more than one thermally accessible level in the temperature range of interest, however a too small separation could result in a switch at extremely low temperature. Therefore, the targeted $\Delta_{0\text{-}1}$ is somewhat intermediate between the desired one for SMM/PCS and MR/OAQB. In practice, this can be achieved exploiting ions with large potential for magnetic anisotropy (*e.g.* lanthanoids) in quasi-spherical coordination environments. Highly symmetrical environments can help in

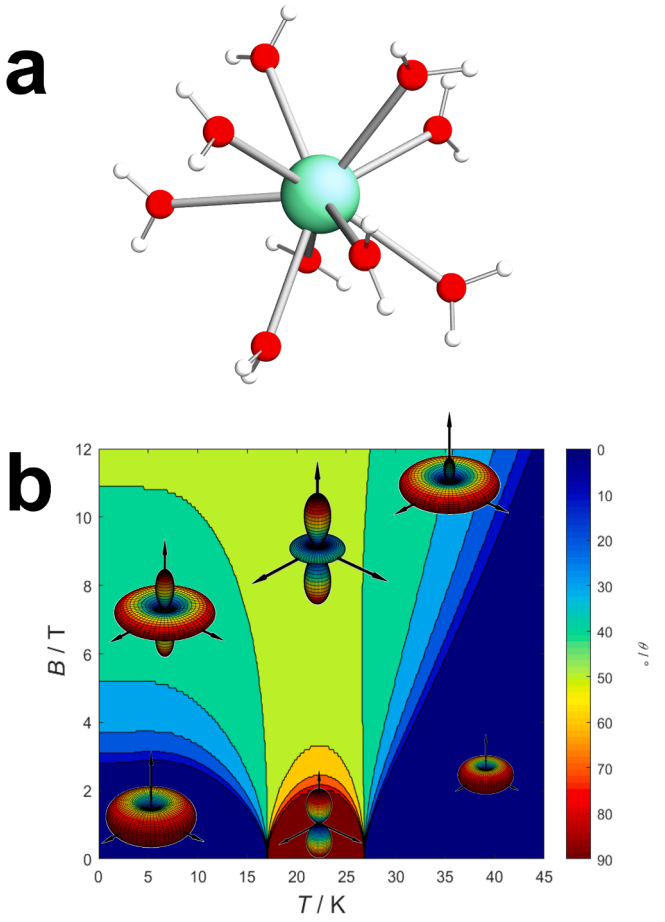

Fig. 11. a) Structure and b) magnetic anisotropy phase diagram of $[Dy(H_2O)_9]^{3+}$ [24]. Colour code: Dy: aquamarine, O: red, H: white.

lowering the mixing of the levels, therefore allowing a higher degree of control. Moreover, since a nontrivial order of the m_J levels is mandatory (*i.e.* not from lowest to highest or *vice versa*) high order Crystal Field parameters are key. For this reason, lanthanoids are well-suited ions while transition metals (especially first row) are not ideal.

Two textbook lanthanoid complexes in this respect are $[PPh_4][Ln[Pt(SAc)_4]_2]$ (Ln = Ho or Er, SAc^-: thioacetate) [201]. The eight oxygen atoms of the two ligands coordinate the lanthanoids in an almost perfect square antiprism fashion. The resulting quasi D4d symmetry favours low mixing and a nontrivial order of the m_J levels. By raising the temperature, the Er-derivative switches anisotropy from easy plane to easy axis at 45 K while the Ho-derivative does the opposite at 18 K. Interestingly, the Pt^{2+} diamagnetic ion in the structure have been replaced with Pd^{2+}, showing that changes in the ligand structure can be exploited to tune the switch and even to quench it, as for $[PPh_4][Dy[M(SAc)_4]_2]$ ($M = Pd^{2+}$ or Pt^{2+}) [32,34].

Moreover, even simple molecules can exhibit complicated magnetic anisotropy diagrams. One such case is the $[Dy(H_2O)_9]^{3+}$ complex, that exhibits a crowded tricapped square prism geometry (Fig. 11a). Indeed, this molecule was theoretically predicted, and experimentally verified to have two switches in temperature [24], as evident from the magnetic anisotropy phase diagram reported in Fig. 11b. A comprehensive overview of molecules exhibiting a switch can be found in the literature [4,24].

3.6. Multifunctional materials

In this review we have shown that the five discussed functional materials can, to a reasonable extent, be designed based on $\Delta_{0\text{-}1}$ and

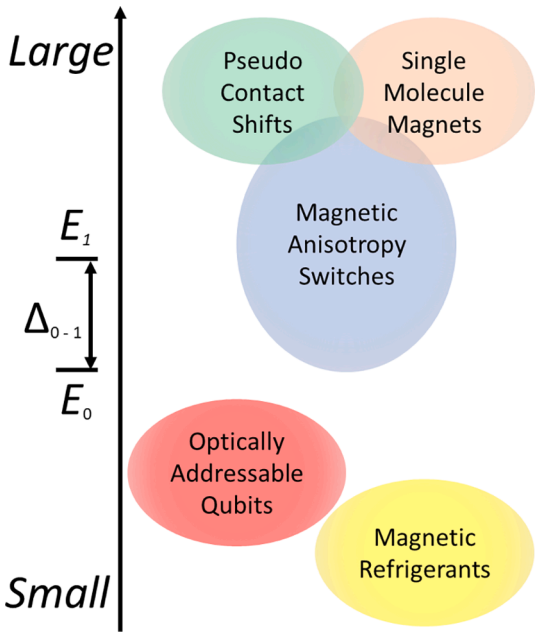

Fig. 12. Classification of the molecular magnetic materials discussed in this paper based on the separation between their ground and first excited state ($\Delta_{0\text{-}1}$).

magnetic anisotropy. A full optimization of each property requires a fine tuning of other material-specific parameters (*e.g.* the relaxation time in SMM or the signal broadening in PCS). Consequently, a complete synergy between two properties is impossible. However, it is often possible to synthesize molecules with several unrelated subunits exhibiting different properties.

If one keeps in mind the required values of the molecular spin, $\Delta_{0\text{-}1}$ and magnetic anisotropy can also be used to assess the possible synergic combinations between different functionalities. In the next paragraphs we focus on multifunctional materials in which the same functional unit is responsible for both properties. Fig. 12 qualitatively summarizes the ideal $\Delta_{0\text{-}1}$ value that must be targeted to obtain a certain material and the degree of overlap between different functionalities.

MR must possess large value of the total spin and extremely small $\Delta_{0\text{-}1}$ to exhibit sizable magnetic entropy changes at low temperature (where the MCE is mostly needed). The first requirement hampers the synergy between MR and OAQB, because OAQB are typically $S = 1$ systems. Moreover, the second requirement is in direct opposition with MAS, PCS and SMM design. To the best of our knowledge, there are no reports of MR + MAS or MR + PCS, but there are several examples of MR + SMM. Typically the combination of these functionalities is obtained in moderately anisotropic metal clusters that are not outstanding SMM [202–204]. A notable exception is the rotating magnetocaloric effect, where an anisotropic single crystal is rotated in a constant magnetic field. For this specific application, good SMM are excellent candidates [195].

OAQB must possess a rather unique electronic structure preventing substantial synergy with the other examined functionalities. Although many SMM have been encoded as electronic [139,205–208] and nuclear [209,210] non-optically addressable qubits, the electronic structure necessary for performing quantum operations in optically addressable systems is substantially at odds with SMM design.

The last three functionalities that we need to discuss are MAS, PCS and SMM. The magnitude of $\Delta_{0\text{-}1}$ in SMM and PCS is very large, while for MAS is usually moderate. However, there is reasonable overlap between

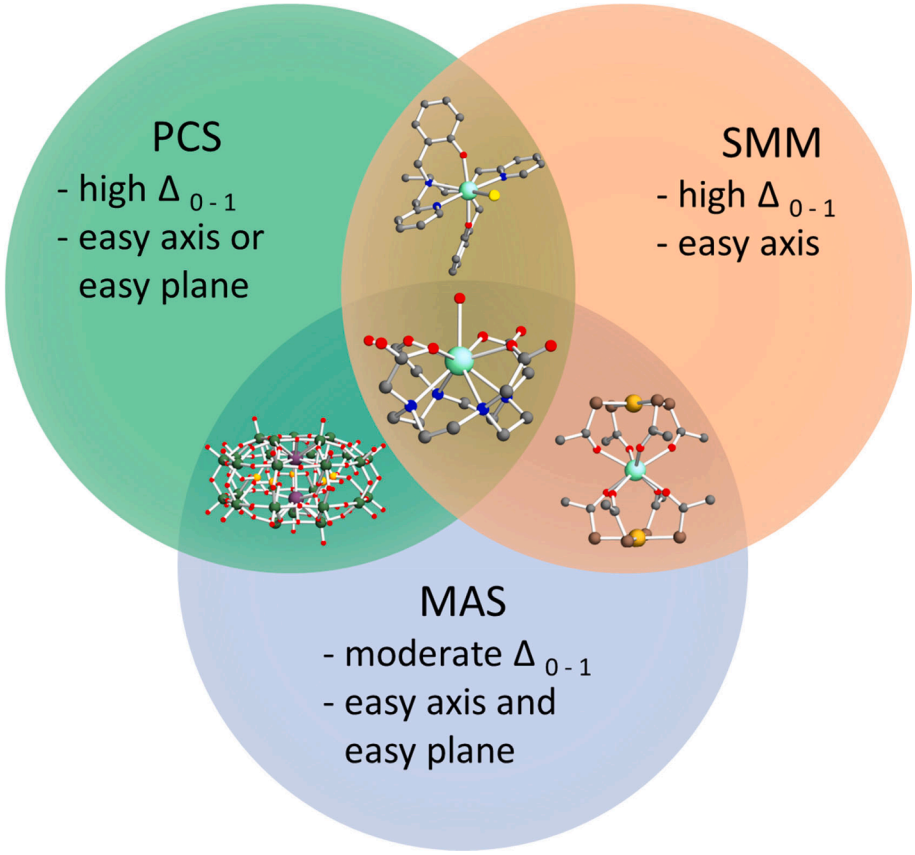

Fig. 13. Pictographic representation of the compatibility between MAS, PCS and SMM properties. The examples discussed in the main text are inserted in the intersections. PCS and SMM: [Dy(bbppn)Cl] [118], PCS and MAS: $[ErW_{30}]$ [211], MAS and SMM: $[Er[Pt(SAc)_4]_2^-$ [32], PCS, MAS and SMM: Dy(DOTA)·H_2O [218]. Colour code: S: brown, O: red, Dy: aquamarine, Pt: light brown C: grey, Cl: yellow, N: blue, Er: violet, W: green, P: orange. H omitted for clarity.

Table 1
Indicative values of $\Delta_{0\text{-}1}$, magnetic anisotropy type required to target the five classes of materials discussed in this paper: Single Molecule Magnets (SMM), Pseudo Contact Shift agents (PCS), Optically Addressable Qubits (OAQB), Magnetic Refrigerants (MR), and Magnetic Anisotropy Switches (MAS) and remarkable examples taken from the literature.

Material	$\Delta_{0\text{-}1}$/cm^{-1}	$\Delta_{0\text{-}1}$ values for some notable examples	Magnetic anisotropy type
SMM	$\gg 100$	$[Co(C(SiMe_2ONaph)_3)_2]$ 468 cm^{-1} [19] $[(Cp^{iPr5})DyCp^*][B(C_6F_5)_4]$ 672 cm^{-1} [84] $[(Cp^{iPr5})_2Dy_2I_3]$ 558 cm^{-1} [90]	Easy axis
PCS	$\gg 100$	[Dy(bbppn)Cl] 405 cm^{-1} [118] $[Tb_2(obPc)_3]$ 370 cm^{-1} [117]	Easy axis better than easy plane
MAS	$5 < \Delta_{0\text{-}1} < 150$	$[YbPc_2]$ 153 cm^{-1} [223] $[PPh_4][Er[Pt(SAc)_4]_2]$ 30 cm^{-1} [201] $[Dy(H_2O)_9][ES]_3$ 8 cm^{-1} [24]	Easy axis *and* easy plane
QB	$0.1 < \Delta_{0\text{-}1} < 5$	$[(C_6F_5)_3trenVCN^tBu]$ 3.6 cm^{-1} [163] $[Ni(phen)_3](BF_4)_2$ 0.9 cm^{-1} [164] $[Cr(o\text{-}tolyl)_4]$ 0.12 cm^{-1} [165]	-
MR	$\ll 1$	Mn_{10} $\approx$0 cm^{-1} [224] $Gd_{12}Na_6$ $\approx$0 cm^{-1} [190]	-

these values, suggesting possible synergy between these functionalities. Fig. 13 shows four molecules that possess a combination of these functionalities.

If the low temperature anisotropy of a MAS is easy axis, it can function as a SMM. At low temperature, the complex $[PPh_4][Dy[Pt(SAc)_4]_2]$ (Fig. 13) has an easy axis magnetic anisotropy and is a SMM [32,34], but the slow relaxation of the magnetization disappears at much lower temperature (<10 K) compared to the switching point at which the magnetic anisotropy becomes easy plane (ca. 120 K). We can argue that for a complete switch (*i.e.* easy axis to easy plane) the switching temperature is an upper limit for the working conditions of a SMM because at such transition the bistability is lost.

The combination MAS + PCS has not yet been reported. However, since the magnetic anisotropy of PCS can be either easy axis or easy plane, many reported MAS could function as PCS. In order to prove this point we have performed a simple calculation using the reported Crystal Field parameters for two polyoxometalate complexes of short formula LnW_{30} (Ln = Er and Tm) [211], that are known to be MAS [24]. The Er-based species switches its anisotropy from easy plane (low temperature) to easy axis (high temperature) while for the Tm species the opposite is true. We must notice that the occurrence of the anisotropy switch below room temperature imposes an anisotropy of the magnetic susceptibility below average for these systems. The value of $\Delta\chi_{ax}$ is, at NMR-compatible experimental conditions (T = 298 K and B = 10 T), 6.0 10^{-33} and $-1.5\ 10^{-33}$ m^3 for ErW_{30} and TmW_{30}, respectively. However, if these molecules were used as PCS agents they would be able to provoke sizable NMR shifts at quite large distances. We calculate that a shift of |0.05| ppm would be experienced by nuclei at 18.5 and 11.7 Å away from the metal centre in ErW_{30} and Tm W_{30}, respectively.

Finally, we discuss perhaps the most synergic combination: SMM + PCS. Such a combination is possible thanks to the common requirement of having large $\Delta_{0\text{-}1}$. The magnetic anisotropy of a SMM must be easy axis, while there is not a strict requirement for the anisotropy of a PCS but, as we have demonstrated in Section 3.2, an easy axis anisotropy is the most convenient also for PCS. However, the operational conditions of these materials are very different: SMM should ideally function when deposited as a solid state array on a surface, while PCS are usually employed in liquid media (typically water) in the presence of biomolecules. This poses stringent constrains regarding the chemical stability, and solubility of the PCS. Unfortunately, the current high performance SMM are solvent, moisture and/or oxygen sensitive. The polydentate bbppn ligand makes Dy(bbppn)Cl a quite robust easy axis magnetic anisotropy building block, although the labile equatorial chlorine atom can be replaced by other ligands, adding some degree of tenability [212–217]. However, the complex is virtually insoluble in water and in fact the outstanding PCSs of Dy(bbppn)Cl were measured in dichloromethane [118]. Summing up, to achieve a SMM and a PCS, one must target a ligand design that boosts an easy axis magnetic anisotropy, keeping in mind that the molecular structure must be robust enough to withstand competing ligands. Functionalized macrocyclic lanthanide complexes with strong axial O-based donors could be an ideal choice.

Finally, we notice that a molecule can even exhibit three of these functionalities (centre of Fig. 13). DyDOTA is a low temperature SMM [218] with the easy axis pointing almost perpendicular to the Dy-OH_2 bond [219–221]. DyDOTA is also recognized as a PCS due to its robust structure in solution [108,124,222]. The magnetic anisotropy of DyDOTA as PCS is close to being of easy plane type. This implies that DyDOTA is also a MAS complex, and it has been indeed demonstrated that its anisotropy switches [125].

4. Conclusions

In this paper we have discussed how the electronic structure and the magnetic anisotropy affect the performances of five types of molecular-based magnetic materials. Our analysis identifies the separation between the ground and the first excited state ($\Delta_{0\text{-}1}$) as an excellent starting point to assess if a material will be more or less suitable for a certain application, as summarized in Fig. 12. Even though exact numbers are difficult to provide, a rough estimation of the best $\Delta_{0\text{-}1}$ and magnetic anisotropy type for each application is specified in Table 1 alongside with $\Delta_{0\text{-}1}$ values extracted from outstanding reported examples. Moreover, our analysis on the chemical structure of the best performance metal complexes present in the literature provide basic guidelines to be used as mainstays for the synthesis of magnetic materials with excellent performances.

Declaration of Competing Interest

The authors declare that they have no known competing financial interests or personal relationships that could have appeared to influence the work reported in this paper.

Data availability

Data will be made available on request.

Acknowledgements

Funded by the European Union (ERC, ELECTRA, 101039890). Views and opinions expressed are however those of the author(s) only and do not necessarily reflect those of the European Union or the European Research Council. Neither the European Union nor the granting authority can be held responsible for them. The financial support provided by the MUR - Dipartimenti di Eccellenza 2023-2027 (DICUS 2.0) to the

Department of Chemistry "Ugo Schiff" of the University of Florence is acknowledged. We thank L. Pattelli (Istituto Nazionale di Ricerca Metrologica), E. Ravera (University of Florence), G. Lorusso (Institute for Microelectronics and Microsystems), and L. Andreis (Politecnico di Milano) for stimulating discussion on simulations. L. Sorace, R. Sessoli, L. Tacconi and C. A. Mattei (University of Florence) are kindly acknowledged for fruitful scientific discussion and proofreading.

References

[1] R. Skomski, Simple Models of Magnetism, Oxford University Press on Demand, 2008.
[2] R. Skomski, D.J. Sellmyer, J. Rare Earths 27 (2009) 675–679.
[3] R. Skomski, J.M.D. Coey, Scr. Mater. 112 (2016) 3–8.
[4] M. Perfetti, J. Bendix, Inorg. Chem. 58 (2019) 11875–11882.
[5] Y.-S. Meng, S.-D. Jiang, B.-W. Wang, S. Gao, Acc. Chem. Res. 49 (2016) 2381–2389.
[6] W.D.W. Horrocks Jr, D.D.W. Hall, Coord. Chem. Rev. 6 (1971) 147–186.
[7] R. Skomski, P. Manchanda, P. Kumar, B. Balamurugan, A. Kashyap, D.J. Sellmyer, IEEE Trans. Magn. 49 (2013) 3215–3220.
[8] A. Aleksashkin, A. Mikkola, Literature Review on Permanent Magnet Generators Design and Dynamic Behavior, Lappenranta University of Technology, 2008.
[9] P. Ryan, E. Diller, IEEE Trans. Rob. 33 (2017) 1398–1409.
[10] I. Mihalcea, M. Perfetti, F. Pineider, L. Tesi, V. Mereacre, F. Wilhelm, A. Rogalev, C.E. Anson, A.K. Powell, R. Sessoli, Inorg. Chem. 55 (2016) 10068–10074.
[11] L. Rigamonti, C. Cotton, A. Nava, H. Lang, T. Rüffer, M. Perfetti, L. Sorace, A. L. Barra, Y. Lan, W. Wernsdorfer, R. Sessoli, A. Cornia, Chem. Eur. J. 22 (2016) 13705–13714.
[12] A. Abragam, B. Bleaney, Electron Paramagnetic Resonance of Transition Ions, Dover, New York, 1986.
[13] C. Rudowicz, C. Chung, J. Phys. Condens. Matter 16 (2004) 5825.
[14] D. Gatteschi, R. Sessoli, J. Villain, Molecular Nanomagnets, Oxford University Press, Oxford, UK, 2006.
[15] M. Perfetti, F. Pointillart, O. Cador, L. Sorace, L. Ouahab, Molecular Magnetic Materials: Concepts and Applications (2016) 345–368.
[16] J. Long, Y. Guari, R.A. Ferreira, L.D. Carlos, J. Larionova, Coord. Chem. Rev. 363 (2018) 57–70.
[17] R. Marx, F. Moro, M. Dörfel, L. Ungur, M. Waters, S.-D. Jiang, M. Orlita, J. Taylor, W. Frey, L. Chibotaru, Chem. Sci. 5 (2014) 3287–3293.
[18] M. Dunstan, R. Mole, C. Boskovic, Eur. J. Inorg. Chem. 8 (2019) 1090–1105.
[19] P.C. Bunting, M. Atanasov, E. Damgaard-Møller, M. Perfetti, I. Crassee, M. Orlita, J. Overgaard, J. van Slageren, F. Neese, J.R. Long, Science 362 (2018) 1378.
[20] M. Perfetti, M. Gysler, Y. Rechkemmer-Patalen, P. Zhang, H. Taştan, F. Fischer, J. Netz, W. Frey, L.W. Zimmermann, T. Schleid, Chem. Sci. 10 (2019) 2101–2110.
[21] J. Van Slageren, New directions in electron paramagnetic resonance spectroscopy on molecular nanomagnets, EPR Spectroscopy: Applications in Chemistry and Biology (2012) 199–234.
[22] A. Schnegg, Emagres (2007) 115–132.
[23] D. Gatteschi, A.L. Barra, A. Caneschi, A. Cornia, R. Sessoli, L. Sorace, Coord. Chem. Rev. 250 (2006) 1514–1529.
[24] M. Perfetti, J. Bendix, Chem. Commun. 54 (2018) 12163–12166.
[25] R. Sessoli, D. Gatteschi, A. Caneschi, M.A. Novak, Nature 365 (1993) 141–143.
[26] S.T. Liddle, J. van Slageren, Chem. Soc. Rev. 44 (2015) 6655–6669.
[27] A. Lunghi, F. Totti, R. Sessoli, S. Sanvito, Nat. Commun. 8 (2017) 14620.
[28] A. Lunghi, F. Totti, S. Sanvito, R. Sessoli, Chem. Sci. 8 (2017) 6051–6059.
[29] M.J. Giansiracusa, A.K. Kostopoulos, D. Collison, R.E. Winpenny, N.F. Chilton, Chem. Commun. 55 (2019) 7025–7028.
[30] A. Castro-Alvarez, Y. Gil, L. Llanos, D. Aravena, Inorg. Chem. Front. 7 (2020) 2478–2486.
[31] D. Reta, J.G. Kragskow, N.F. Chilton, J. Am. Chem. Soc. 143 (2021) 5943–5950.
[32] M.A. Sørensen, U.B. Hansen, M. Perfetti, K.S. Pedersen, E. Bartolomé, G. G. Simeoni, H. Mutka, S. Rols, M. Jeong, I. Zivkovic, M. Retuerto, A. Arauzo, J. Bartolomé, S. Piligkos, H. Weihe, L.H. Doerrer, J. van Slageren, H.M. Rønnow, K. Lefmann, J. Bendix, Nat. Commun. 9 (2018) 1292.
[33] J.J. Baldoví, S. Cardona-Serra, J.M. Clemente-Juan, E. Coronado, A. Gaita-Ariño, A. Palii, Inorg. Chem. 51 (2012) 12565–12574.
[34] N.A. Bonde, J.B. Petersen, M.A. Sørensen, U.G. Nielsen, B.r. Fåk, S. Rols, J. Ollivier, H. Weihe, J. Bendix, M. Perfetti, Inorg. Chem. 59 (2019) 235–243.
[35] L. Ungur, L. Chibotaru, Inorg. Chem. 55 (2016) 10043–10056.
[36] K. Irländer, J. Schnack, Phys. Rev. B 102 (2020), 054407.
[37] F. Ortu, D. Reta, Y.-S. Ding, C.A. Goodwin, M.P. Gregson, E.J. McInnes, R. E. Winpenny, Y.-Z. Zheng, S.T. Liddle, D.P. Mills, N. Chilton, Dalton Trans. 48 (2019) 8541–8545.
[38] Y.-S. Ding, K.-X. Yu, D. Reta, F. Ortu, R.E. Winpenny, Y.-Z. Zheng, N.F. Chilton, Nat. Commun. 9 (2018) 1–10.
[39] S.G. McAdams, A.-M. Ariciu, A.K. Kostopoulos, J.P. Walsh, F. Tuna, Coord. Chem. Rev. 346 (2017) 216–239.
[40] G. Aromí, E.K. Brechin, Synthesis of 3d metallic single-molecule magnets, in: Single-molecule magnets and related phenomena, Springer, 2006, pp. 1–67.
[41] N. Magnani, R. Caciuffo, Inorganics 6 (2018) 26.
[42] J. Ferrando-Soria, J. Vallejo, M. Castellano, J. Martinez-Lillo, E. Pardo, J. Cano, I. Castro, F. Lloret, R. Ruiz-Garcia, M. Julve, Coord. Chem. Rev. 339 (2017) 17–103.
[43] K. Chakarawet, P.C. Bunting, J.R. Long, J. Am. Chem. Soc. 140 (2018) 2058–2061.
[44] C.J. Milios, A. Vinslava, W. Wernsdorfer, S. Moggach, S. Parsons, S.P. Perlepes, G. Christou, E.K. Brechin, J. Am. Chem. Soc. 129 (2007) 2754–2755.
[45] C.J. Milios, R. Inglis, A. Vinslava, R. Bagai, W. Wernsdorfer, S. Parsons, S. P. Perlepes, G. Christou, E.K. Brechin, J. Am. Chem. Soc. 129 (2007) 12505–12511.
[46] S. Accorsi, A.L. Barra, A. Caneschi, G. Chastanet, A. Cornia, A.C. Fabretti, D. Gatteschi, C. Mortalo, E. Olivieri, F. Parenti, P. Rosa, R. Sessoli, L. Sorace, W. Wernsdorfer, L. Zobbi, J. Am. Chem. Soc. 128 (2006) 4742–4755.
[47] S. Nayak, M. Evangelisti, A.K. Powell, J. Reedijk, Chem. Eur. J. 16 (2010) 12865–12872.
[48] O. Waldmann, Inorg. Chem. 46 (2007) 10035–10037.
[49] K.E. Marriott, L. Bhaskaran, C. Wilson, M. Medarde, S.T. Ochsenbein, S. Hill, M. Murrie, Chem. Sci. 6 (2015) 6823–6828.
[50] Y.-Y. Zhu, C. Cui, Y.-Q. Zhang, J.-H. Jia, X. Guo, C. Gao, K. Qian, S.-D. Jiang, B.-W. Wang, Z.-M. Wang, Chem. Sci. 4 (2013) 1802–1806.
[51] Y. Rechkemmer, F.D. Breitgoff, M. Van Der Meer, M. Atanasov, M. Hakl, M. Orlita, P. Neugebauer, F. Neese, B. Sarkar, J. Van Slageren, Nat. Commun. 7 (2016) 10467–10475.
[52] X.-N. Yao, J.-Z. Du, Y.-Q. Zhang, X.-B. Leng, M.-W. Yang, S.-D. Jiang, Z.-X. Wang, Z.-W. Ouyang, L. Deng, B.-W. Wang, S. Gao, J. Am. Chem. Soc. 139 (2017) 373–380.
[53] P.E. Kazin, M.A. Zykin, L.A. Trusov, A.A. Eliseev, O.V. Magdysyuk, R. E. Dinnebier, R.K. Kremer, C. Felser, M. Jansen, Chem. Commun. 53 (2017) 5416–5419.
[54] J.M. Zadrozny, D.J. Xiao, M. Atanasov, G.J. Long, F. Grandjean, F. Neese, J. R. Long, Nature Chem. (2013).
[55] Z. Zhu, J. Tang, Natl. Sci. Rev. 9 (2022) nwac194.
[56] J.D. Rinehart, J.R. Long, Chem. Sci. 2 (2011) 2078–2085.
[57] J. Sievers, Z. Phys. B: Condens. Matter 45 (1982) 289–296.
[58] Y.C. Chen, J.L. Liu, W. Wernsdorfer, D. Liu, L.F. Chibotaru, X.M. Chen, M.L. Tong, Angew. Chem. Int. Ed. 56 (2017) 4996–5000.
[59] Z. Zhu, C. Zhao, T. Feng, X. Liu, X. Ying, X.-L. Li, Y.-Q. Zhang, J. Tang, J. Am. Chem. Soc. 143 (2021) 10077–10082.
[60] Y.S. Ding, N.F. Chilton, R.E. Winpenny, Y.Z. Zheng, Angew. Chem. 128 (2016) 16305–16308.
[61] J. Long, A.O. Tolpygin, E. Mamontova, K.A. Lyssenko, D. Liu, M.D. Albaqami, L. F. Chibotaru, Y. Guari, J. Larionova, A.A. Trifonov, Inorg. Chem. Front. 8 (2021) 1166–1174.
[62] X.L. Ding, Y.Q. Zhai, T. Han, W.P. Chen, Y.S. Ding, Y.Z. Zheng, Chem. Eur. J. 27 (2021) 2623–2627.
[63] L. Zhu, Y. Dong, B. Yin, P. Ma, D. Li, Dalton Trans. 50 (2021) 12607–12618.
[64] J. Long, A.O. Tolpygin, D.M. Lyubov, N.Y. Rad'kova, A.V. Cherkasov, Y. V. Nelyubina, Y. Guari, J. Larionova, A.A. Trifonov, Dalton Trans. 50 (2021) 8487–8496.
[65] A.B. Canaj, S. Dey, E.R. Martí, C. Wilson, G. Rajaraman, M. Murrie, Angew. Chem. Int. Ed. 58 (2019) 14146–14151.
[66] A.B. Canaj, S. Dey, C. Wilson, O. Céspedes, G. Rajaraman, M. Murrie, Chem. Commun. 56 (2020) 12037–12040.
[67] S. Liu, Y. Gil, C. Zhao, J. Wu, Z. Zhu, X.-L. Li, D. Aravena, J. Tang, Inorg. Chem. Front. 9 (2022) 4982–4989.
[68] C. Zhao, Z. Zhu, X.-L. Li, J. Tang, Inorg. Chem. Front. 9 (2022) 4049–4055.
[69] P. Zhang, L. Zhang, C. Wang, S. Xue, S.-Y. Lin, J. Tang, J. Am. Chem. Soc. 136 (2014) 4484–4487.
[70] S.-D. Jiang, B.-W. Wang, H.-L. Sun, Z.-M. Wang, S. Gao, J. Am. Chem. Soc. 133 (2011) 4730–4733.
[71] J.D. Hilgar, M.G. Bernbeck, J.D. Rinehart, J. Am. Chem. Soc. 141 (2019) 1913–1917.
[72] A.P. Orlova, J.D. Hilgar, M.G. Bernbeck, M. Gembicky, J.D. Rinehart, J. Am. Chem. Soc. 144 (2022) 11316–11325.
[73] J.J. Le Roy, L. Ungur, I. Korobkov, L.F. Chibotaru, M. Murugesu, J. Am. Chem. Soc. 136 (2014) 8003–8010.
[74] W. Cai, J.D. Bocarsly, A. Gomez, R.J.L. Lee, A. Metta-Magana, R. Seshadri, L. Echegoyen, Chem. Sci. 11 (2020) 13129–13136.
[75] L. Spree, A.A. Popov, Dalton Trans. 48 (2019) 2861–2871.
[76] F. Liu, D.S. Krylov, L. Spree, S.M. Avdoshenko, N.A. Samoylova, M. Rosenkranz, A. Kostanyan, T. Greber, A.U. Wolter, B. Büchner, A.A. Popov, Nat. Commun. 8 (2017) 16098.
[77] C.A. Goodwin, F. Ortu, D. Reta, N.F. Chilton, D.P. Mills, Nature 548 (2017) 439–442.
[78] R. Layfield, F.-S. Guo, B. Day, Y.-C. Chen, M.-L. Tong, A. Mansikamäkki, Angew. Chem. Int. Ed. 56 (2017) 11445–11449.
[79] P. Evans, D. Reta, G.F. Whitehead, N.F. Chilton, D.P. Mills, J. Am. Chem. Soc. 141 (2019) 19935–19940.
[80] K.R. McClain, C.A. Gould, K. Chakarawet, S.J. Teat, T.J. Groshens, J.R. Long, B. G. Harvey, Chem. Sci. 9 (2018) 8492–8503.
[81] L. Muenzfeld, C. Schoo, S. Bestgen, E. Moreno-Pineda, R. Köppe, M. Ruben, P. W. Roesky, Nat. Commun. 10 (2019) 3135.
[82] J.P. Durrant, B.M. Day, J. Tang, A. Mansikkamäki, R.A. Layfield, Angew. Chem. Int. Ed. 134 (2022) e202200525.
[83] J.C. Vanjak, B.O. Wilkins, V. Vieru, N.S. Bhuvanesh, J.H. Reibenspies, C. D. Martin, L.F. Chibotaru, M. Nippe, J. Am. Chem. Soc. 144 (2022) 17743–17747.
[84] F.-S. Guo, B.M. Day, Y.-C. Chen, M.-L. Tong, A. Mansikkamäki, R.A. Layfield, Science 362 (2018) 1400–1403.
[85] A.H. Vincent, Y.L. Whyatt, N.F. Chilton, J.R. Long, J. Am. Chem. Soc. (2023).

[86] Z. Zhu, J. Tang, Chem. Soc. Rev. (2022).
[87] T. Pugh, N.F. Chilton, R.A. Layfield, Angew. Chem. Int. Ed. 55 (2016) 11082–11085.
[88] D. Krylov, F. Liu, S. Avdoshenko, L. Spree, B. Weise, A. Waske, A. Wolter, B. Büchner, A. Popov, Chem. Commun. 53 (2017) 7901–7904.
[89] R.J. Blagg, L. Ungur, F. Tuna, J. Speak, P. Comar, D. Collison, W. Wernsdorfer, E. J. McInnes, L.F. Chibotaru, R.E. Winpenny, Nat. Chem. 5 (2013) 673–678.
[90] C.A. Gould, K.R. McClain, D. Reta, J.G. Kragskow, D.A. Marchiori, E. Lachman, E.-S. Choi, J.G. Analytis, R.D. Britt, N.F. Chilton, B.G. Harvey, J.R. Long, Science 375 (2022) 198–202.
[91] S. Demir, I.-R. Jeon, J.R. Long, T.D. Harris, Coord. Chem. Rev. 289 (2015) 149–176.
[92] P. Zhang, R. Nabi, J.K. Staab, N.F. Chilton, S. Demir, J. Am. Chem. Soc. (2023).
[93] C.A. Gould, L.E. Darago, M.I. Gonzalez, S. Demir, J.R. Long, Angew. Chem. Int. Ed. 56 (2017) 10103–10107.
[94] C.A. Gould, E. Mu, V. Vieru, L.E. Darago, K. Chakarawet, M.I. Gonzalez, S. Demir, J.R. Long, J. Am. Chem. Soc. 142 (2020) 21197–21209.
[95] P. Zhang, Q.C. Luo, Z. Zhu, W. He, N. Song, J. Lv, X. Wang, Q.G. Zhai, Y.Z. Zheng, J. Tang, Angew. Chem. Int. Ed. 62 (2023) e202218540.
[96] J.D. Rinehart, M. Fang, W.J. Evans, J.R. Long, J. Am. Chem. Soc. 133 (2011) 14236–14239.
[97] S. Demir, M. Nippe, M.I. Gonzalez, J.R. Long, Chem. Sci. 5 (2014) 4701–4711.
[98] S. Demir, J.M. Zadrozny, M. Nippe, J.R. Long, J. Am. Chem. Soc. 134 (2012) 18546–18549.
[99] N. Mavragani, A.A. Kitos, J.L. Brusso, M. Murugesu, Chem. Eur. J. 27 (2021) 5091–5106.
[100] J.D. Rinehart, M. Fang, W.J. Evans, J.R. Long, Nature Chem. 3 (2011) 538–542.
[101] S. Demir, M.I. Gonzalez, L.E. Darago, W.J. Evans, J.R.J.N.c. Long, Giant coercivity and high magnetic blocking temperatures for N23− radical-bridged dilanthanide complexes upon ligand dissociation, Nat. Commun. 8 (2017) 2144.
[102] J.T. Coutinho, M.A. Antunes, L.C. Pereira, H. Bolvin, J. Marçalo, M. Mazzanti, M. Almeida, Dalton Trans. 41 (2012) 13568–13571.
[103] J.T. Coutinho, M. Perfetti, J.J. Baldoví, M.A. Antunes, P.P. Hallmen, H. Bamberger, I. Crassee, M. Orlita, M. Almeida, J. van Slageren, L.C. Pereira, Chem. Eur. J. 25 (2019) 1758–1766.
[104] C. Apostolidis, A. Kovács, O. Walter, E. Colineau, J.C. Griveau, A. Morgenstern, J. Rebizant, R. Caciuffo, P.J. Panak, T. Rabung, B. Schimmelpfennig, M. Perfetti, Chem. Eur. J. 26 (2020) 11293–11306.
[105] F.S. Guo, Y.C. Chen, M.L. Tong, A. Mansikkamäki, R.A. Layfield, Angew. Chem. Int. Ed. 131 (2019) 10269–10273.
[106] V. Mougel, L. Chatelain, J. Pécaut, R. Caciuffo, E. Colineau, J.-C. Griveau, M. Mazzanti, Nature Chem. 4 (2012) 1011–1017.
[107] L. Chatelain, J.P. Walsh, J. Pécaut, F. Tuna, M. Mazzanti, Angew. Chem. 126 (2014) 13652–13656.
[108] E. Ravera, L. Gigli, L. Fiorucci, C. Luchinat, G. Parigi, Phys. Chem. Chem. Phys. 24 (2022) 17397–17416.
[109] T. Müntener, D. Joss, D. Häussinger, S. Hiller, Chem. Rev. 122 (2022) 9422–9467.
[110] L. Banci, I. Bertini, K. Bren, M. Cremonini, H. Gray, C. Luchinat, P. Turano, J. Biol. Inorg. Chem. 1 (1996) 117–126.
[111] D.J. Crick, J.X. Wang, B. Graham, J.D. Swarbrick, H.R. Mott, D. Nietlispach, J. Biomol. NMR 61 (2015) 197–207.
[112] J. Li, K.B. Pilla, Q. Li, Z. Zhang, X. Su, T. Huber, J. Yang, J. Am. Chem. Soc. 135 (2013) 8294–8303.
[113] U. Brath, S.I. Swamy, A.X. Veiga, C.-C. Tung, F. Van Petegem, M. Erdélyi, J. Am. Chem. Soc. 137 (2015) 11391–11398.
[114] C. Göbl, M. Resch, M. Strickland, C. Hartlmüller, M. Viertler, N. Tjandra, T. Madl, Angew. Chem. Int. Ed. 55 (2016) 14847–14851.
[115] T. Muntener, D. Häussinger, P. Selenko, F.-X. Theillet, J. Phys. Chem. Lett. 7 (2016) 2821–2825.
[116] H.M. McConnell, J. Chem. Phys. 27 (1957) 226–229.
[117] M. Damjanovic, K. Katoh, M. Yamashita, M. Enders, J. Am. Chem. Soc. 135 (2013) 14349–14358.
[118] F.S. Santana, M. Perfetti, M. Briganti, F. Sacco, G. Poneti, E. Ravera, J.F. Soares, R. Sessoli, Chem. Sci. 13 (2022) 5860–5871.
[119] Y.Z. Voloshin, V.V. Novikov, Y.V. Nelyubina, RSC advances 5 (2015) 72621–72637.
[120] O.A. Varzatskii, L.V. Penkova, S.V. Kats, A.V. Dolganov, A.V. Vologzhanina, A. A. Pavlov, V.V. Novikov, A.S. Bogomyakov, V.N. Nemykin, Y.Z. Voloshin, Inorg. Chem. (Washington, DC, U. S.) 53 (2014) 3062–3071.
[121] O.A. Varzatskii, S.V. Kats, A.A. Pavlov, A.S. Belov, I.G. Belaya, Y.V. Nelyubina, V. V. Novikov, Y.Z. Voloshin, Inorg. Chim. Acta 471 (2018) 413–418.
[122] A.C. Harnden, D. Parker, N.J. Rogers, Coord. Chem. Rev. 383 (2019) 30–42.
[123] E.A. Suturina, K. Mason, C.F. Geraldes, N.F. Chilton, D. Parker, I. Kuprov, Phys. Chem. Chem. Phys. 20 (2018) 17676–17686.
[124] M. Marques, C. Geraldes, A. Sherry, A.E. Merbach, H. Powell, D. Pubanz, S. Aime, M. Botta, J. Alloys Compd. 225 (1995) 303–307.
[125] M. Briganti, E. Lucaccini, L. Chelazzi, S. Ciattini, L. Sorace, R. Sessoli, F. Totti, M. Perfetti, J. Am. Chem. Soc. 143 (2021) 8108–8115.
[126] Y. Kobashigawa, T. Saio, M. Ushio, M. Sekiguchi, M. Yokochi, K. Ogura, F. Inagaki, J. Biomol. NMR 53 (2012) 53–63.
[127] M. Atzori, R. Sessoli, J. Am. Chem. Soc. 141 (2019) 11339–11352.
[128] W.K. Wootters, W.H. Zurek, Nature 299 (1982) 802–803.
[129] H.J. Kimble, Nature 453 (2008) 1023–1030.
[130] S. Wehner, D. Elkouss, R. Hanson, Science 362 (2018) eaam9288.
[131] D.W. Laorenza, D.E. Freedman, J. Am. Chem. Soc. 144 (2022) (1825) 21810–21812.
[132] D.P. DiVincenzo, Fortschritte der Phys. 48 (2000) 771–783.
[133] G. Fuchs, G. Burkard, P. Klimov, D. Awschalom, Nat. Phys. 7 (2011) 789–793.
[134] S. Hernández-Gómez, N. Fabbri, Front. Phys. 8 (2021), 610868.
[135] G. Wendin, Rep. Prog. Phys. 80 (2017), 106001.
[136] M.H. Devoret, R.J. Schoelkopf, Science 339 (2013) 1169–1174.
[137] J. You, F. Nori, Phys. Today 58 (2005) 42.
[138] W. Pfaff, B.J. Hensen, H. Bernien, S.B. van Dam, M.S. Blok, T.H. Taminiau, M. J. Tiggelman, R.N. Schouten, M. Markham, D.J. Twitchen, Science 345 (2014) 532–535.
[139] A. Gaita-Ariño, F. Luis, S. Hill, E. Coronado, Nature Chem. 11 (2019) 301–309.
[140] M.J. Graham, J.M. Zadrozny, M.S. Fataftah, D.E. Freedman, Chem. Mater. 29 (2017) 1885–1897.
[141] S. Nakazawa, S. Nishida, T. Ise, T. Yoshino, N. Mori, R.D. Rahimi, K. Sato, Y. Morita, K. Toyota, D. Shiomi, M. Kitagawa, H. Hara, P. Carl, P. Höfer, T. Takui, Angew. Chem. Int. Ed. 51 (2012) 9860–9864.
[142] A. Urtizberea, E. Natividad, P.J. Alonso, L. Pérez-Martínez, M.A. Andrés, I. Gascón, I. Gimeno, F. Luis, O. Roubeau, Mat. Horiz. 7 (2020) 885–897.
[143] C.-J. Yu, S. Von Kugelgen, M.D. Krzyaniak, W. Ji, W.R. Dichtel, M.R. Wasielewski, D.E. Freedman, Chem. Mater. 32 (2020) 10200–10206.
[144] L. Tesi, E. Lucaccini, I. Cimatti, M. Perfetti, M. Mannini, M. Atzori, E. Morra, M. Chiesa, A. Caneschi, L. Sorace, R. Sessoli, Chem. Sci. 7 (2016) 2074–2083.
[145] D. Ranieri, F. Santanni, A. Privitera, A. Albino, E. Salvadori, M. Chiesa, F. Totti, L. Sorace, R. Sessoli, Chem. Sci. 14 (2022) 61–69.
[146] S.J. Lockyer, A. Chiesa, A. Brookfield, G.A. Timco, G.F. Whitehead, E.J. McInnes, S. Carretta, R.E. Winpenny, J. Am. Chem. Soc. 144 (2022) 16086–16092.
[147] M. Chizzini, L. Crippa, A. Chiesa, F. Tacchino, F. Petiziol, I. Tavernelli, P. Santini, S. Carretta, Phys. Rev. Res. 4 (2022), 043135.
[148] M. Atzori, L. Tesi, E. Morra, M. Chiesa, L. Sorace, R. Sessoli, J. Am. Chem. Soc. 138 (2016) 2154–2157.
[149] J.M. Zadrozny, J. Niklas, O.G. Poluektov, D.E. Freedman, A.C.S. Cent, Sci. 1 (2015) 488–492.
[150] T. Takui, L. Berliner, G. Hanson, Electron Spin Resonance (ESR) Based Quantum Computing, Springer, 2016.
[151] M.J. Graham, M.D. Krzyaniak, M.R. Wasielewski, D.E. Freedman, Inorg. Chem. 56 (2017) 8106–8113.
[152] M.J. Graham, C.-J. Yu, M.D. Krzyaniak, M.R. Wasielewski, D.E. Freedman, J. Am. Chem. Soc. 139 (2017) 3196–3201.
[153] R. Sessoli, Nature 548 (2017) 400–401.
[154] M.S. Fataftah, J.M. Zadrozny, S.C. Coste, M.J. Graham, D.M. Rogers, D. E. Freedman, J. Am. Chem. Soc. 138 (2016) 1344–1348.
[155] J.M. Zadrozny, J. Niklas, O.G. Poluektov, D.E. Freedman, J. Am. Chem. Soc. 136 (2014) 15841–15844.
[156] J.M. Zadrozny, A.T. Gallagher, T.D. Harris, D.E. Freedman, J. Am. Chem. Soc. 139 (2017) 7089–7094.
[157] M. Zhong, M.P. Hedges, R.L. Ahlefeldt, J.G. Bartholomew, S.E. Beavan, S. M. Wittig, J.J. Longdell, M.J. Sellars, Nature 517 (2015) 177–180.
[158] F. Jelezko, T. Gaebel, I. Popa, A. Gruber, J. Wrachtrup, Phys. Rev. Lett. 92 (2004), 076401.
[159] A.L. Falk, B.B. Buckley, G. Calusine, W.F. Koehl, V.V. Dobrovitski, A. Politi, C. A. Zorman, P.-X.-L. Feng, D.D. Awschalom, Nat. Commun. 4 (2013) 1–7.
[160] W.F. Koehl, B. Diler, S.J. Whiteley, A. Bourassa, N.T. Son, E. Janzén, D. D. Awschalom, Phys. Rev. B 95 (2017), 035207.
[161] M.S. Fataftah, D.E. Freedman, Chem. Commun. 54 (2018) 13773–13781.
[162] S. Bayliss, D. Laorenza, P. Mintun, B. Kovos, D. Freedman, D. Awschalom, Science 370 (2020) 1309–1312.
[163] M.S. Fataftah, S.L. Bayliss, D.W. Laorenza, X. Wang, B.T. Phelan, C.B. Wilson, P. J. Mintun, B.D. Kovos, M.R. Wasielewski, S. Han, J. Am. Chem. Soc. 142 (2020) 20400–20408.
[164] M.K. Wojnar, D.W. Laorenza, R.D. Schaller, D.E. Freedman, J. Am. Chem. Soc. 142 (2020) 14826–14830.
[165] D.W. Laorenza, A. Kairalapova, S.L. Bayliss, T. Goldzak, S.M. Greene, L.R. Weiss, P. Deb, P.J. Mintun, K.A. Collins, D.D. Awschalom, J. Am. Chem. Soc. 143 (2021) 21350–21363.
[166] S. Bayliss, P. Deb, D. Laorenza, M. Onizhuk, G. Galli, D. Freedman, D. Awschalom, Phys. Rev. X 12 (2022), 031028.
[167] B.A. Glowacki, W.J. Nuttall, R.H. Clarke, IEEE Trans. Appl. Supercond. 23 (2013), 0500113-0500113.
[168] G. Ventura, M. Perfetti, Thermal Properties of Solids at Room and Cryogenic Temperatures, Springer, 2014.
[169] R.A. Kishore, S. Priya, Sustainable Energy and Fuels 1 (2017) 1899–1908.
[170] R.L. Carlin, Magnetochemistry, Springer Science & Business Media, 2012.
[171] V. Franco, J. Blázquez, J. Ipus, J. Law, L. Moreno-Ramírez, A. Conde, Prog. Mat. Sci. 93 (2018) 112–232.
[172] M. Evangelisti, E.K. Brechin, Dalton Trans. 39 (2010) 4672–4676.
[173] A.M. Tishin, Y.I. Spichkin, The Magnetocaloric Effect and its Applications, CRC Press, 2016.
[174] V.K. Pecharsky, K.A. Gschneidner, J. Magn. Magn. Mater. 200 (1999) 44–56.
[175] J.-L. Liu, Y.-C. Chen, F.-S. Guo, M.-L. Tong, Coord. Chem. Rev. 281 (2014) 26–49.
[176] P. Konieczny, W. Sas, D. Czernia, A. Pacanowska, M. Fitta, R. Pełka, Dalton Trans. 51 (2022) 12762–12780.
[177] M. Evangelisti, F. Luis, L.J. De Jongh, M. Affronte, J. Mater. Chem. 16 (2006) 2534–2549.
[178] Y.C. Chen, F.S. Guo, J.L. Liu, J.D. Leng, P. Vrábel, M. Orendáč, J. Prokleška, V. Sechovský, M.L. Tong, Chem. Eur. J. 20 (2014) 3029–3035.
[179] M. Evangelisti, O. Roubeau, E. Palacios, A. Camón, T.N. Hooper, E.K. Brechin, J. J. Alonso, Angew. Chem. Int. Ed. 50 (2011) 6606–6609.

[180] X. Zhong, J.-J. Hu, S.-L. Yao, R.-J. Zhang, J.-J. Wang, D.-G. Cai, T.-K. Luo, Y. Peng, S.-J. Liu, H.-R. Wen, CrystEngComm (2022) 7861–7868.
[181] G. Lorusso, J.W. Sharples, E. Palacios, O. Roubeau, E.K. Brechin, R. Sessoli, A. Rossin, F. Tuna, E.J. McInnes, D. Collison, Adv. Mater. (Weinheim, Germany) 25 (2013) 4653–4656.
[182] Q.-F. Xu, B.-L. Liu, M.-Y. Ye, L.-S. Long, L.-S. Zheng, Inorg. Chem. 60 (2021) 9259–9262.
[183] M. Andruh, J.-P. Costes, C. Diaz, S. Gao, Inorg. Chem. 48 (2009) 3342–3359.
[184] E. Colacio, J. Ruiz, G. Lorusso, E.K. Brechin, M. Evangelisti, Chem. Commun. 49 (2013) 3845–3847.
[185] Y. Tang, W. Guo, S. Zhang, M. Yang, H. Xiang, Z. He, Dalton Trans. 44 (2015) 17026–17029.
[186] S.-J. Liu, X.-R. Xie, T.-F. Zheng, J. Bao, J.-S. Liao, J.-L. Chen, H.-R. Wen, CrystEngComm 17 (2015) 7270–7275.
[187] A. Adhikary, H.S. Jena, S. Konar, Dalton Trans. 44 (2015) 15531–15543.
[188] N. Ahmed, C. Das, S. Vaidya, A.K. Srivastava, S.K. Langley, K.S. Murray, M. Shanmugam, Dalton Trans. 43 (2014) 17375–17384.
[189] X.-M. Luo, Z.-B. Hu, Q.-F. Lin, W. Cheng, J.-P. Cao, C.-H. Cui, H. Mei, Y. Song, Y. Xu, J. Am. Chem. Soc. 140 (2018) 11219–11222.
[190] T.G. Tziotzi, D. Gracia, S.J. Dalgarno, J.r. Schnack, M. Evangelisti, E.K. Brechin, C.J. Milios,, J. Am. Chem. Soc. (2023).
[191] W.-P. Chen, P.-Q. Liao, P.-B. Jin, L. Zhang, B.-K. Ling, S.-C. Wang, Y.-T. Chan, X.-M. Chen, Y.-Z. Zheng, J. Am. Chem. Soc. 142 (2020) 4663–4670.
[192] J.W. Sharples, D. Collison, E.J. McInnes, J. Schnack, E. Palacios, M. Evangelisti, Nat. Commun. 5 (2014) 1–6.
[193] J. Schnack, R. Schmidt, J. Richter, Phys. Rev. B 76 (2007), 054413.
[194] M. Perfetti, Coord. Chem. Rev. 348 (2017) 171–186.
[195] G. Lorusso, O. Roubeau, M. Evangelisti, Angew. Chem. Int. Ed. 128 (2016) 3421–3424.
[196] P. Konieczny, R. Pełka, E. Kuźniak, R. Podgajny, J. Magn. Magn. Mater. 563 (2022), 170001.
[197] P. Konieczny, D. Czernia, T. Kajiwara, Sci. Rep. 12 (2022) 1–10.
[198] K. Engelbrecht, D. Eriksen, C. Bahl, R. Bjørk, J. Geyti, J. Lozano, K.K. Nielsen, F. Saxild, A. Smith, N. Pryds, Int. J. Refrig. 35 (2012) 1498–1505.
[199] F. El Hallak, P. Rosa, P. Vidal, I. Sheikin, M. Dressel, J. Van Slageren, Europhys. Lett. 95 (2011) 57002.
[200] O. Waldmann, L. Zhao, L.K. Thompson, Phys. Rev. Lett. 88 (2002), 066401.
[201] M. Perfetti, M.A. Sørensen, U.B. Hansen, H. Bamberger, S. Lenz, P.P. Hallmen, T. Fennell, G.G. Simeoni, A. Arauzo, J. Bartolomé, E. Bartolomé, K. Lefmann, H. Weihe, J. van Slageren, J. Bendix, Adv. Funct. Mater. 32 (2018) 1801846.
[202] X.X. Zhang, H.L. Wei, Z.Q. Zhang, L.Y. Zhang, Phys. Rev. Lett. 87 (2001).
[203] F. Torres, J.M. Hernandez, X. Bohigas, J. Tejada, Appl. Phys. Lett. 77 (2000) 3248–3250.
[204] M. Evangelisti, A. Candini, A. Ghirri, M. Affronte, E.K. Brechin, E.J.L. Mcinnes, Appl. Phys. Lett. 87 (2005), 072504.
[205] E. Moreno-Pineda, C. Godfrin, F. Balestro, W. Wernsdorfer, M. Ruben, Chem. Soc. Rev. 47 (2018) 501–513.
[206] E. Moreno-Pineda, W. Wernsdorfer, Nat. Rev. Phys. 3 (2021) 645–659.
[207] D. Aguila, L.A. Barrios, V. Velasco, O. Roubeau, A. Repollés, P.J. Alonso, J. Sesé, S.J. Teat, F. Luis, G. Aromí, J. Am. Chem. Soc. 136 (2014) 14215–14222.
[208] M. Jenkins, Y. Duan, B. Diosdado, J.J. García-Ripoll, A. Gaita-Ariño, C. Giménez-Saiz, P.J. Alonso, E. Coronado, F. Luis, Phys. Rev. B 95 (2017), 064423.
[209] C. Godfrin, A. Ferhat, R. Ballou, S. Klyatskaya, M. Ruben, W. Wernsdorfer, F. Balestro, Phys. Rev. Lett. 119 (2017), 187702.
[210] M. Shiddiq, D. Komijani, Y. Duan, A. Gaita-Ariño, E. Coronado, S. Hill, Nature 531 (2016) 348–351.
[211] S. Cardona-Serra, J. Clemente-Juan, E. Coronado, A. Gaita-Ariño, A. Camón, M. Evangelisti, F. Luis, M. Martínez-Pérez, J. Sesé, J. Am. Chem. Soc. 134 (2012) 14982–14990.
[212] Y. Dong, L. Zhu, B. Yin, X. Zhu, D. Li, Dalton Trans. 50 (2021) 17328–17337.
[213] Y. Yamada, D. Koori, K. Mori, Y. Oshikawa, J. Coord. Chem. 69 (2016) 3735–3744.
[214] S. Zhang, W. Mo, B. Yin, X. Lü, J. Zhang, New J. Chem. 43 (2019) 454–462.
[215] T. Gregório, J.d.M. Leão, G.A. Barbosa, J.d.L. Ramos, S. Om Kumar Giese, M. Briganti, P.C. Rodrigues, E.L. de Sá, E.R. Viana, D.L. Hughes, L.D. Carlos, R.A. S. Ferreira, A.G. Macedo, G.G. Nunes, S.J. F, Inorg. Chem. 58 (2019) 12099–12111.
[216] S. Zhang, J. Tang, J. Zhang, F. Xu, S. Chen, D. Hu, B. Yin, J. Zhang, Inorg. Chem. 60 (2021) 816–830.
[217] J. Liu, Y.-C. Chen, J.-L. Liu, V. Vieru, L. Ungur, J.-H. Jia, L.F. Chibotaru, Y. Lan, W. Wernsdorfer, S. Gao, X.-M. Chen, M.-L. Tong, J. Am. Chem. Soc. 138 (2016) 5441–5450.
[218] P.E. Car, M. Perfetti, M. Mannini, A. Favre, A. Caneschi, R. Sessoli, Chem. Commun. 47 (2011) 3751–3753.
[219] G. Cucinotta, M. Perfetti, J. Luzon, M. Etienne, P.E. Car, A. Caneschi, G. Calvez, K. Bernot, R. Sessoli, Angew. Chem. Int. Ed. 51 (2012) 1606–1610.
[220] M.E. Boulon, G. Cucinotta, J. Luzon, C. Degl'Innocenti, M. Perfetti, K. Bernot, G. Calvez, A. Caneschi, R. Sessoli, Angew. Chem. Int. Ed. 125 (2013) 368–372.
[221] M. Briganti, G.F. Garcia, J. Jung, R. Sessoli, B. Le Guennic, F. Totti, Chem. Sci. (2019).
[222] D. Cicolari, F. Santanni, L. Grassi, F. Brero, M. Filibian, T. Recca, P. Arosio, M. Perfetti, M. Mariani, R. Sessoli, A. Lascialfari, J. Chem. Phys. 155 (2021), 214201.
[223] N. Ishikawa, M. Sugita, T. Okubo, N. Tanaka, T. Lino, Y. Kaizu, Inorg. Chem. 42 (2003) 2440–2446.
[224] M. Manoli, R.D.L. Johnstone, S. Parsons, M. Murrie, M. Affronte, M. Evangelisti, E.K. Brechin, Angew. Chem. Int. Ed. 46 (2007) 4456–4460.